TAMPEREEN TEKNILLINEN YLIOPISTO
TAMPERE UNIVERSITY OF TECHNOLOGY

HOSSEIN SAGHLATOON

INKJET PRINTED CIRCUITS ON FIBROUS SUBSTRATES FOR ENVIRONMENTALLY-FRIENDLY RADIO-FREQUENCY ELECTRONICS APPLICATIONS

Master of Science Thesis

Examiners: Professor Leena Ukkonen
and Professor LauriSydänheimo
Examiner and topic approved by the
Council of the Faculty of Computing
and Electrical Engineering on
April 2014

ABSTRACT

TAMPERE UNIVERSITY OF TECHNOLOGY
Master's Degree Programme in the Faculty of Computing and Electrical Engineering
SAGHLATOON, HOSSEIN: Inkjet Printed circuits on Fibrous Substrates for Environmentally-Friendly Radio-Frequency Electronics Applications
Master of Science Thesis, 58 pages
April 2014
Major: Radio Frequency Electronics
Examiner: Professor Leena Ukkonen and Professor Lauri Sydänheimo
Keywords: Environmentally friendly electronics, Fibrous paper based substrate, Inkjet printing, Power harvesting, Wideband planar monopole antenna,

Additive printing technology like inkjet printing provides the ability to increase the circuit fabrication speed and possibility to implement the desired circuit on unconventional substrates such as wood and paper. It is tempting to utilize paper based substrate in the realization of electronic devices since it is really low-cost, recyclable, available everywhere and compatible with inkjet printing technology. The fabrication of environmentally-friendly and low-cost products is one of the main goals in any manufacturing fields which might not be feasible using every technologies or techniques. This demand can be fulfilled by exploiting paper as the substrate and inkjet printing as the fabrication technique. Moreover, power consumed by a device is one of the most important parameters especially for wireless and mobile applications. Power consumption reduction is a really challenging procedure in many circuits; thus, preparing the desired supply power from useless sources can be a practical alternative. The absorption of the energy of the useless transmitted electromagnetics signals in different frequency bands is so called power-harvesting.

In this project the whole procedure in order to fabricate an antenna for the power-harvesting application using inkjet printing technology on fibrous paper based substrate has been investigated. For this purpose electrical parameters of cardboard and silver ink which are used as the substrate and conductor, respectively, were extracted. Then, according to the demands the required antenna was designed, simulated and fabricated.

PREFACE

The master thesis, “Inkjet Printed Circuits on Fibrous Substrates for Environmentally-Friendly Radio-Frequency Electronics Applications”, was done in partial fulfilment of the requirement for the Master of Science degree in Radio Frequency Electronics major, in the Department of Electronics and Communications Engineering at Tampere University of Technology. All the researches and investigations have been done in the Wireless Identification and Sensing Systems Research Group (WISE) under the supervision of Prof. Leena Ukkonen and Prof. Lauri Sydänheimo.

I would like to thank my thesis examiners and supervisors, Prof. Leena Ukkonen and Prof. Lauri Sydänheimo for all of their supports, guidance and for providing me an appropriate environment to complete my thesis. I am also thankful to all my colleagues in the WISE Group for their help and support.

Moreover, I would like to express my appreciation to my lovely wife, Maliheh Soleimani, for her patience and endless support through all the time of my studies.

Finally, I would like to thank my great parents for all their love, prayers, teaching and motivations through my life.

Tampere, April 2014

Hossein Saghlatoon

TABLE OF CONTENTS

ABBREVIATIONS

A	Ampere
AR	Axial Ratio
EM	Electromagnetic
E-Plane	A two-dimensional representation of the radiation pattern which contains only electric field and maximum radiation direction.
cm	centimetre
dB	decibel
DC	Direct Current
DOD	Drop-On-Demand
DPI	Dot Per Inch
DW	Direct Writing
EMC	Electromagnetic Compatibility
fL	femto Liter
GHz	Giga Hertz
GND	Ground Plane
HPBW	Half Power Beam Width
H-Plane	A two-dimensional representation of the radiation pattern which contains only magnetic field and maximum radiation direction.
Hz	Hertz
Im	Imaginary part of a complex number
KHz	Kilo Hertz
MHz	Mega Hertz
mm	millimetre
nL	nano Liter
pL	pico Liter
Q	Quality Factor
Re	Real part of a complex number
RF	Radio Frequency
S	Siemens
SOLT	Short-Open-Load-Thru
S-Parameters	Scattering Parameters
SWR	Standing Wave Ratio
TRL	Through-Line-Reflection
UV	Ultra Violet
V	Volt
VNA	Vector Network Analyzer
Wb	Weber
wt%	Percent by weight

2D	Two Dimensional
3D	Three Dimensional
µm	micrometre
Ω	Ohm

SYMBOLS

c	Speed of light [m/s]
B	Magnetic flux density [Wb/m^2]
C	Capacitance per unit length [F/m]
D	Electric displacement [C/m^2]
D	Directivity of antenna [dBi]
E	Electric field [V/m]
F	Electric force [N]
G	Conductance per unit length [S/m]
G	Gain of antenna [dBi]
f	Frequency [Hz]
H	Magnetic field [A/m]
$I(z)$	Current wave in z direction [A]
J	Current density [A/m^2]
k	Radiation efficiency of antenna
L	Inductance per unit length [H/m]
L_{RL}	Return loss [dB]
M	Vector magnetization [A/m]
P	Vector polarization [C/m^2]
Q	Electric charge [C]
R	Resistance per unit length [Ω/m]
R_A	Resistance of antenna [Ω]
$tan\delta$	Loss tangent
$V(z)$	Voltage wave in z direction [V]
W_e	Electric energy [J]
W_m	Magnetic energy [J]
X_A	Reactance of antenna [Ω]
Z_0	Characteristic impedance [Ω]
Z_A	Impedance of antenna [Ω]
α	Attenuation constant [Np/m]
α_c	Conductor loss constant [Np/m]
α_d	Dielectric loss constant [Np/m]
α_r	Radiation loss constant [Np/m]
β	Propagation constant [Np/m]
γ	Complex propagation constant [Np/m]
Γ	Reflection coefficient
δ	Skin depth [m]
ε	Permittivity
ε_r	Relative permittivity
ε_0	Permittivity of free space
ε_{eff}	Effective relative permittivity

μ	Permeability
μ_r	Relative permeability
μ_0	Permeability of free space
ρ	Electric charge density [C/m^3]
σ	Conductivity [S/m]
ω	Angular frequency [rad/s]

1. INTRODUCTION

Paper has a great potential for the fabrication of environmentally-friendly and recyclable electronics besides the advantages of being low-cost, available everywhere and compatible with printing procedure [1], [2], [3]. From mass production point of view fabrication speed, production versatility and the total implementation cost are critical features which can be improved by the utilization of inkjet-printing technology. In addition, the inkjet-printing technique can be used to fabricate electronic circuits on unconventional substrates such as wood, ceramic and paper [3], [4], [5]. In order to design a circuit for RF/Microwave frequencies, the properties of substrate such as permittivity, loss tangent and thickness, and properties of conductor like conductivity and thickness should be known. Since the main application of paper based substrates is not for implementation of circuits, these parameters should be investigated first.

Harvesting the useless part of the transmitted electromagnetics signals has a great potential for energizing low power electronic wireless communications circuits in future [6]. The harvesting system is utilized to absorb the signals in different frequency bands and provide the required energy for driving electronic devices. The general idea is to reduce the power consumption by providing the energy from useless sources in the environment [7].

In this thesis one typical cardboard paper material is used as the substrate, and silver nanoparticle ink as the conductor. In the Chapter 2, the essential information as the background for electromagnetics theory discussed. Basics of antennas theory is covered in the Chapter 3 while the inkjet-printing technology is introduced in the Chapter 4. The Chapter 5 includes the theoretical and experimental studies on the characterization of the substrate and conductor as well as surface treatment and improvement of the conductivity. The obtained values from the investigations proposed in this section are utilized to design a patch antenna and band stop filter in the same chapter in order to convey the reliability of the model. Finally, in the Chapter 6 a wideband planar monopole antenna is proposed and fabricated for power-harvesting application.

2. ELECTROMAGNETICS THEORY

In order to understand the basic phenomena of antennas and radio frequency (RF) circuits, it is essential to study the electromagnetics theory. For this purpose the electric and magnetic fields should be surveyed separately then, using Maxwell's equations the properties of electromagnetics wave can be investigated. In this chapter the study of electromagnetics theory begins with the discussion about electric and magnetic fields, pursues with Maxwell's equations and completes by representing the concept of the plane wave.

2.1 Electric Field

In electrostatic situation in which the charges are at rest and there are no time variant fields, the study case is simple. In this condition, electric field (V/m) can be defined as the force (N) per unit electric charge (C). Using equation (2.1) it can be seen that the strength of the electric filed depends on the amount of the electric charge and the distance from it. The electric force can be obtained by Coulomb's law which is represented in equation (2.2),

$$E = \frac{F}{Q} = \frac{Q}{4\pi\varepsilon r^2}\hat{r} \qquad (2.1)$$

$$F = \frac{Q_1 Q_2}{4\pi\varepsilon r^2}\hat{r} \qquad (2.2)$$

where Q_i is the electric charge, ε is the electric permittivity of the medium and r is the distance from the electric charge. The curl and divergence of electric field in free space for electrostatic condition can be specified using equation (2.3) and equation (2.4),

$$\nabla . E = \frac{\rho}{\varepsilon} \qquad (2.3)$$

$$\nabla \times E = 0 \qquad (2.4)$$

$$\varepsilon = \varepsilon_0 \varepsilon_r \qquad (2.5)$$

where ρ (C/m^3) is the volume charge density, and ε is the electric permittivity of the medium which can be calculated by utilizing equation (2.5) in which ε_0 is the permittivity of free space and ε_r the relative permittivity of the medium.

When a dielectric body is placed in an external electric field, each atom aligns in the direction of the field and forms a microscopic dipole. This phenomenon is called polarization of the dielectric material which modifies the electric field inside and outside of the dielectric. The superposition of the microscopic polarization vectors forms the vec-

tor polarization P (C/m^2). Accordingly the electric flux density or electric displacement D (C/m^2) can be defined by equation (2.6).

$$D = \varepsilon_0 E + P = \varepsilon E \quad (2.6)$$

2.2 Magnetic Field

In magnetostatic situation in which only we have time invariant current, we can only consider the magnetic flux density B (Wb/m^2) described with curl and divergence in free space using the equations (2.7) and (2.8),

$$\nabla . B = 0 \quad (2.7)$$

$$\nabla \times B = \mu_0 J \quad (2.8)$$

where μ_0 is the magnetic permeability of free space and J is the current density 0 [9]. When there is an external magnetic field in the medium, the moving electrical charges experience a force which can be expressed by equation (2.9),

$$F = qu \times B \quad (2.9)$$

where q is the electric charge and u is the velocity vector of electrical charges.

Alike the electric field, when a body is place in an external magnetic field, the magnetic moments of spinning electrons are aligned and a magnetic moment is induced due to the change in the orbital motion of electrons. This phenomenon is so called magnetization of the material. The superposition of these microscopic magnetic moments forms the magnetization vector M. Using the definition of the magnetization it is feasible to define magnetic field intensity H (A/m) which is represented by equation (2.10),

$$H = \frac{B}{\mu_0} - M = \frac{B}{\mu} \quad (2.10)$$

where μ is the permeability of the medium. [9]

2.3 Maxwell's Equations

Maxwell's equations consist of four equations which define the relationships between magnetic field, electric field, electric charge and electric current in general case when there is time variation in the parameters. These equations are expressed using equations (2.11) to (2.14) [10]. These equations are known independently as Faraday's law of induction (2.11), Ampere's circuital law (2.12), Gauss's law for electric fields (2.13) and Gauss's law for magnetic fields (2.14).

$$\nabla \times E = -\frac{\partial B}{\partial t} - M \quad (2.11)$$

$$\nabla \times H = J + \frac{\partial D}{\partial t} \quad (2.12)$$

$$\nabla . D = \rho \quad (2.13)$$

$$\nabla . B = 0 \qquad (2.14)$$

In order to solve general electromagnetic problems Maxwell's equations, equations (2.6), (2.10) and (2.15) are enough. In equation (2.15), σ is the conductivity of the material.

$$J = \sigma E \qquad (2.15)$$

2.4 Wave Equations

If the electric and magnetic fields time dependency is $e^{j\omega t}$, it is possible to represent Maxwell's equations in phasor form. In linear, isotropic, homogeneous region, Maxwell's curl equation can be expressed as equations (2.16) and (2.17) [10].

$$\nabla \times \overline{E} = -j\omega\mu\overline{H} \qquad (2.16)$$

$$\nabla \times \overline{H} = j\omega\varepsilon\overline{E} + \sigma\overline{E} \qquad (2.17)$$

By taking the curl of equations (2.16) and (2.17), substitute each one in the other one, and then simplifying them using equation (2.19) Helmholtz equations expressed in equations (2.20) and (2.21) can be obtained. For a source free region ρ is equal to zero. The solutions of these equations in source free medium for one dimension are represented in equations (2.22) and (2.23) which are in phasor domain and time domain, respectively.

$$\nabla \times \nabla \times \overline{E} = -j\omega\mu\nabla \times \overline{H} = \omega^2\mu\varepsilon\overline{E} \qquad (2.18)$$

$$\nabla \times \nabla \times A = \nabla(\nabla . A) - \nabla^2 A \qquad (2.19)$$

$$\nabla^2\overline{E} + \omega^2\mu\varepsilon\left(1 - j\frac{\sigma}{\omega\varepsilon}\right)\overline{E} = \nabla(\frac{\rho}{\varepsilon}) \qquad (2.20)$$

$$\nabla^2\overline{H} + \omega^2\mu\varepsilon\left(1 - j\frac{\sigma}{\omega\varepsilon}\right)\overline{H} = 0 \qquad (2.21)$$

$$E(z) = E^+e^{-\gamma z} + E^-e^{\gamma z} \qquad (2.22)$$

$$E(z,t) = Ee^{-\alpha z}\cos(\omega t - \beta z) \qquad (2.23)$$

where γ is the complex propagation constant for the medium and can be expressed by equation (2.24),

$$\gamma = \alpha + j\beta = j\omega\sqrt{\mu\varepsilon}\sqrt{a - j\frac{\sigma}{\omega\varepsilon}} \qquad (2.24)$$

where α is the attenuation constant and β is the propagation constant [10].

2.5 Plane Wave

A particular solution of Maxwell's equations in which *E* field (similarly for *H*) is in the same direction, same value, and same phase in planes perpendicular to the direction of propagation is so called plane wave. In addition, in a plane EM wave, *E* field and *H*

field are perpendicular to each other as well as the propagation direction. In other words, *E* and *H* fields have components only in the transverse plane. If the plane wave is propagated in a loss-less medium, its amplitude stays constant, α=0 and γ is purely imaginary. If the medium is a lossy dielectric, then σ=0 but ε is complex, hence α≠0 and the amplitude decreases while the wave propagates. In order to represent the loss of a dielectric medium, loss tangent (*tanδ*) is usually utilized which is the ratio between the imaginary part of permittivity and the real part. If the medium is a good conductor then σ>>ωε and the magnitude of the wave decreases by the propagation in this medium. For expressing the conductor loss skin depth (δ_s) is exploited which can be seen in equation (2.25),

$$\delta_s = \frac{1}{\alpha} = \sqrt{\frac{2}{\omega\mu\sigma}} \qquad (2.25)$$

where ω is the angular frequency of the wave. If the propagation medium is a perfect conductor the EM wave cannot propagate inside. [10]

The polarization of the EM wave is the time-varying behavior of the electric field vector at a given point in space which can be categorized in three different types of linear, circular and elliptical polarizations [11]. In linear polarization *E* field vector varies only in one direction while in elliptical and circular polarization it has components in two dimensions. Axial ratio is the ratio of the major to minor field vector in the transvers plane and describes the polarization situation. This parameter can have a value between 1 and ∞, for circular polarization its value is 1, for linear polarization it is ∞, and for elliptical polarization it is between these two values [11]. The different polarization categories are depicted in Figure 2.1.

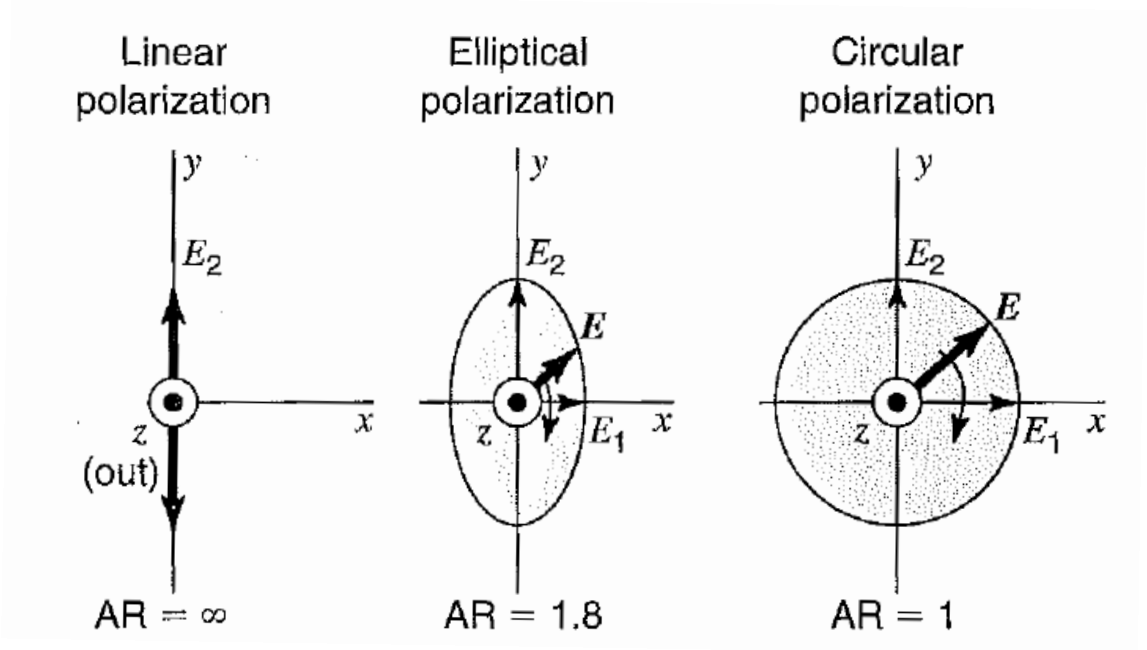

(a) (b) (c)

Figure 2.1. Different polarization types. (a) Linear, (b) elliptical, and (c) circular polarization [11].

2.6 Energy and Power

A source of electromagnetic energy produces fields such that they store energy in electric and magnetic forms and carry power. In steady state sinusoidal situation, the stored energy in electric form in volume *V* can be obtained by equation (2.26) [10].

$$W_e = \frac{1}{4} Re \int_V \overline{E}.\overline{D}^* dv \qquad (2.26)$$

Similarly the magnetic energy stored in volume *V* can be defined by (2.27) [10].

$$W_m = \frac{1}{4} Re \int_V \overline{H}.\overline{B}^* dv \qquad (2.27)$$

The complex power delivered by the sources inside the volume *V* can be calculated as

$$P_s = -\frac{1}{2} \int_V \left(\overline{E}.\overline{J}_s^{\,*} + \overline{H}.\overline{M}_s^{\,*}\right) dv, \qquad (2.28)$$

where J_s and M_s are the sources inside the volume *V* [10].

The complex power flow out of the boundary of the volume *V* can be calculated as

$$P_o = \frac{1}{2} \oint_S \overline{E} \times \overline{H}^* ds, \qquad (2.29)$$

where *S* is the closed surface surrounds the volume *V* [10].

The power dissipated inside the volume *V* can be expressed as

$$P_l = \frac{\sigma}{2} \int_V |\overline{E}|^2 dv + \frac{\omega}{2} \int_V (Im(\varepsilon)\left|\overline{E}\right|^2 + Im(\mu)\left|\overline{H}\right|^2) dv \qquad (2.30)$$

Using the above definition it is possible to define the Poyning's theorem as [10]

$$P_s = P_o + P_l + 2j\omega(W_m + W_e) \qquad (2.31)$$

which states that the power delivered by the sources inside the volume *V* is equal to the summation of the power dissipated inside the volume, power transmitted through the boundaries of the volume, and 2ω times of the reactive energy stored in the electric and magnetic fields inside the volume [10].

2.7 Transmission Line

If the physical dimensions of a circuit are comparable with the wavelength of the signal, it is not feasible to analyze the circuit using the circuit theory; therefore, the transmission line theory should be utilized. In the transmission line theory the elements of the circuit are distributed along the line, but in order to solve the circuit parameters lumped-element equivalent circuit shown in Figure 2.2 is assumed for a very short length of the circuit. The circuit parameters like voltage and current are solved using circuit theory for this short segment and finally the general solution for these parameters along the line is obtained.

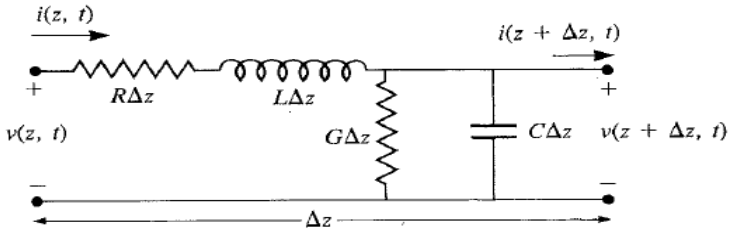

Figure 2.2. The lumped-element equivalent circuit for a short segment of a transmission line [10].

The general solution of two wave equations obtained for voltage and current of the transmission line according to the aforementioned procedure are represented in equations (2.32) and (2.33),

$$V(z) = V_0^+ e^{-\gamma z} + V_0^- e^{\gamma z} \quad (2.32)$$

$$I(z) = I_0^+ e^{-\gamma z} + I_0^- e^{\gamma z} \quad (2.33)$$

where

$$\gamma = \alpha + j\beta = \sqrt{(R + j\omega L)(G + j\omega C)} \quad (2.34)$$

is the complex propagation constant, R is series resistance per unit length, L is series inductance per unit length, G is shunt conductance per unit length, and C is shunt capacitance per unit length [10]. The impedance of the line (Z_0) can be described by equation (2.35).

$$Z_0 = \frac{V_0^+}{I_0^+} = -\frac{V_0^-}{I_0^-} = \sqrt{\frac{(R+j\omega L)}{(G+j\omega C)}} \quad (2.35)$$

When a transmission line is terminated to an arbitrary load, the wave reflection occurs in the load location. The ratio of the incident voltage to incident current is Z_0, while in the load this ratio should be Z_L. Thus a reflected wave should appear in order to fulfil the continuity of voltage wave [10]. In order to deduce the reflection, the voltage reflection coefficient Γ is defined as

$$\Gamma = \frac{V_0^-}{V_0^+} = \frac{Z_L - Z_0}{Z_L + Z_0} \quad (2.36)$$

The superposition of the incident wave and reflected one make a standing wave along the transmission line which is terminated to a mismatch load ($Z_L \neq Z_0$). The other parameter which can be used to describe the reflection is standing wave ratio (SWR) explained by equation [10].

$$SWR = \frac{V_{max}}{V_{min}} = \frac{1+|\Gamma|}{1-|\Gamma|} \quad (2.37)$$

2.8 Scattering Parameters

There are many different parameters utilized for explaining the operation of a circuit by using the network ports parameters such as impedance parameter (Z-Parameters), admittance (Y-Parameters), ABCD and scattering (S-Parameters). These parameters explain the relationship between the input and output voltages and currents of a network

[10]. By increasing the operation frequency it is not practical to use Z,Y and ABCD parameters since for finding them, voltages and currents are needed. Measuring voltages and currents directly with voltmeter and ampere meter is not feasible, thus for measurement only S-parameters are used. The measurement of S-parameters can be done by measuring the incident and reflected power. The scattering parameters can be defined according to the incident and reflected voltage at ports using equation (2.38)

$$S_{ij} = \frac{V_i^-}{V_j^+} \ (when\ V_k^+ = 0\ for\ k \neq j), \qquad (2.38)$$

where i and j are the indices for the ports of network. Equation (2.39) represents the same definition with power parameters.

$$S_{ij} = \frac{b_i}{a_j} \ (when\ a_k = 0\ for\ k \neq j), \qquad (2.39)$$

where b_i is the reflected power from port i and a_j is the incident power at port j [10].

2.9 Microstrip Line

Microstrip line is a planar transmission line which is appropriate to be fabricated using photolithography, etching and printing. Figure 2.3 illustrates the geometry of a conventional microstrip line. The thickness and relative permittivity of the substrate is d and ε_r, respectively, and the width of the line is W [10].

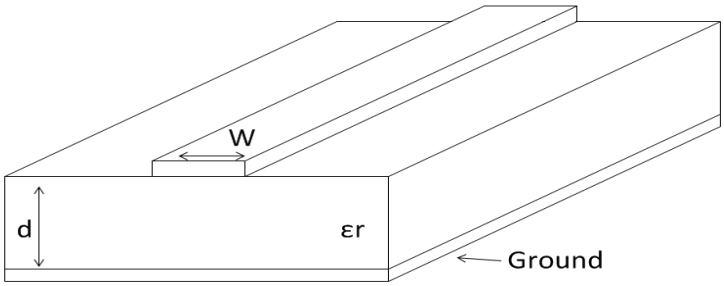

Figure 2.3. The geometry of microstrip line.

Since part of the fields propagates inside the substrate and the rest propagate in the air the equivalent permittivity of the combination of the substrate and air can be approximated using equation (2.40).

$$\varepsilon_{eff} = \frac{\varepsilon_r+1}{2} + \frac{\varepsilon_r-1}{2}\frac{1}{\sqrt{1+12\frac{d}{W}}} \qquad (2.40)$$

3. BASIC THEORY OF ANTENNA

An antenna is a passive component which starts to radiate when a signal is inserted to its input ports and the signal appears in it port when a radio wave is captured by the antenna. It is a transition between the transmission line and free space and converts electrons to photons and vice versa [11]. It is utilized to transmit and receive radio waves [12]. In order to study the antennas, the parameters which define antenna performance should be explained first. Radiation patterns, bandwidth, half power beam width (HPBW), directivity and gain, return loss, efficiency, polarization and axial ratio are among the most important practical parameters. Antennas can be categories as wire antenna, aperture antenna, patch antenna, reflector antenna and lens antenna with different performances and applications [12].

3.1 How an Antenna Radiates

When there is a time-variant current distribution in the antenna structure, the acceleration and deceleration of the electric charges produce time-variant *E* and *H* fields around the antenna which propagate in all directions [11]. The characteristics of these fields are different with respect to the distance from the antenna. The space surrounding the antenna can be divided in three main regions which are reactive near-field, radiating near-field (Fresnal), and far-field (Fraunhofer) regions [12]. In the far-field region the propagated radio wave can be assumed as plane wave.

3.2 Antennas Parameters

There are different parameters of antenna which should be considered to design proper antenna. By exploiting these parameters it is feasible to compare different antennas for the desired applications. Following are the basic parameters of antennas.

3.2.1 Radiation Pattern

The radiated field by the antenna has a three-dimensional (3D) spatial pattern which is called the radiation pattern. In order to represent the radiation characteristics of the antenna two fundamental patterns are illustrated which are E-plane and H-plane. The E-plane is a plane contains the electric field vector and the direction of the maximum radiation, while the H-plane contains the magnetic field vector and the direction of the max-

imum radiation [12]. Figure 3.1 depicts the representation of E-plane and H-plane for an aperture antenna. Usually, the radiation patterns are illustrated in polar coordinates.

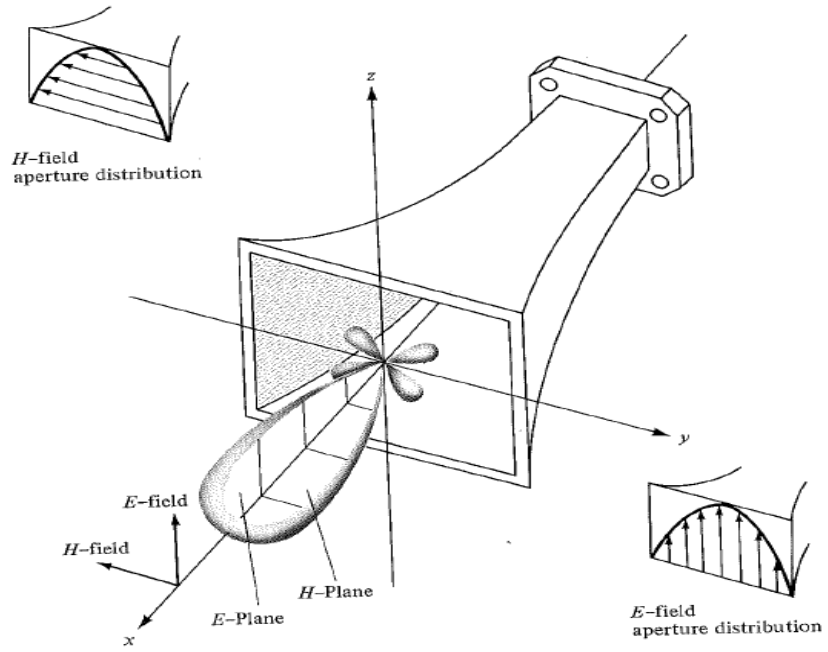

Figure 3.1. The representation of E-plane and H-plane of an aperture antenna [12].

3.2.2 Half Power Beam Width (HPBW)

The radiation patterns of an antenna can be divided into different sections such as main lobe, side lobes, back lobes, minor lobes and nulls. The angle between the points in the main lobe in which the magnitude of the radiated power is half of the pick value is called HPBW [13]. Figure 3.2 illustrates a typical radiation pattern, its different parts and the concept of HPBW.

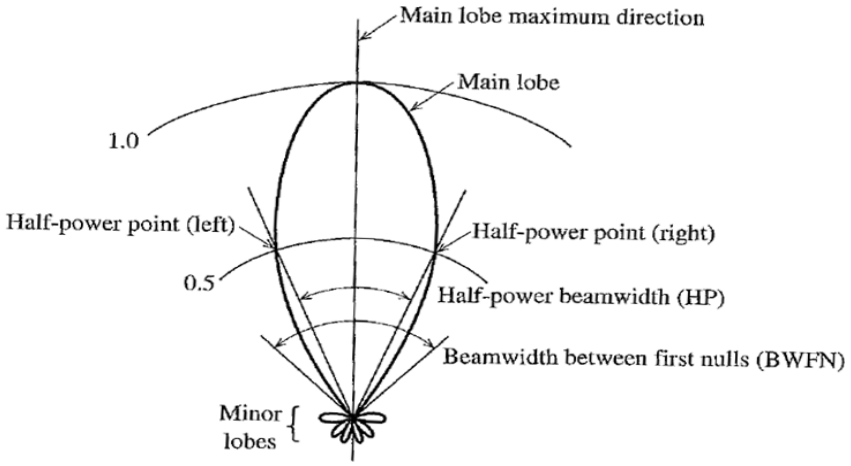

Figure 3.2. The illustration of a typical radiation pattern with its different sections [13].

3.2.3 Directivity and Gain

The directivity *D* and gain *G* are among the most important parameters of an antenna [11]. The ratio of the maximum power density P_{max}(W/m^2) to the average value P_{av} (W/m^2) is the directivity of an antenna. The gain of an antenna is the same as directivity while the effect of antenna efficiency (*k*) is also included. The mathematical expression for the directivity, gain and efficiency of an antenna are expressed as

$$D = \frac{P_{max}}{P_{av}} \quad (3.1)$$

$$G = kD \quad (3.2)$$

$$k = \frac{P_{rad}}{P_{in}} = \frac{P_{rad}}{P_{rad}+P_{loss}} \quad (3.3)$$

where P_{rad} is the radiated power by the antenna and P_{loss} is the power dissipation because of the ohmic losses of the antenna [11]. Usually the gain of an antenna is referred in logarithmic scale. Thus, the definition can be the ratio of the gain of antenna to the gain of the isotropic antenna (which radiates identically in all direction) or to the gain of the dipole antenna. In the first case the unit of the gain is dBi and in the second case it is dBd.

$$G(dBi) = 10\log\left(\frac{G}{G_{iso}}\right) = 10\log(G) \quad (3.4)$$

$$G(dBd) = 10\log\left(\frac{G}{G_{dipole}}\right) = 10\log(\frac{G}{1.64}) \quad (3.5)$$

3.2.4 Input Impedance and Return Loss

The impedance of an antenna is the impedance seen from the antenna terminals and consists of real and imaginary parts which is shown in equation (3.6). The real part represents the losses and radiations of the antenna, while the imaginary part shows the energy stored in the near-field of antenna [13].

$$Z_A = R_A + jX_A = (R_{rad} + R_{loss}) + jX_A \quad (3.6)$$

Return loss or reflection loss represents the reflection of the signal when the transmission line is connected to a load or device. A reflection occurs because of discontinuity and mismatch and degrades the amount of power delivered to the load. Thus, its behavior can be modeled as a loss phenomenon. The concept of return loss can be demonstrated using equation (3.7). [10]

$$L_{RL}(dB) = -20\log(\Gamma_{in}) \quad (3.7)$$

3.2.5 Bandwidth

The bandwidth of an antenna is the frequency range in which antenna operates properly. Usually, 10 dB return loss bandwidth is utilized to explain the performance of the an-

tenna in frequency spectrum. In this definition the return loss of the antenna is higher than 10 dB in the whole frequency band [12].

3.2.6 Polarization and Axial Ratio

The polarization of an antenna is the polarization of the radiated EM wave. Depends on the application antennas are designed to have either linear or circular polarization [11]. Aforementioned axial ratio is a parameter describes the quality of polarization.

4. INKJET-PRINTING TECHNOLOGY

Whenever there is a discussion regarding to implementation of a circuit, one of the most important issues is related to the fabrication procedure which affects the cost, reliability and performance of the system [14]. There are various methods to implement a circuit such as photolithography and direct printing. There are some challenges regarding the utilization of photolithography consists of great amount of waste, many different fabrication steps and quality of printed circuit [14]. On the other hand, the fabrication process using direct printing technology is capable of low-cost mass production, exploitation of unconventional substrate like wood and paper, and low material wastage. There are various types of direct writing (DW) procedure which can be categorized in four main groups. They are droplet-based DW, energy beam-based DW, flow-based DW and tip-based DW methods [15]. Droplet-based DW method can be divided into two main groups: inkjet and aerosol, where the inkjet technology is the most common method and can be utilized as continuous or drop-on-demand (DOD) [15]. In DOD individual nuzzles in array format generate single drop of ink, by excitation of a transient pressure pulse. In this method drops are ejected only when they are needed to be printed and they are formed by the print head by thermal, piezoelectric, electrostatic or acoustic excitation [14]. In the piezoelectric method, as shown in Figure 4.1 the ink is poured into a cavity which is inside the print head and ejected when the voltage pulse deforms the piezoelectric material.

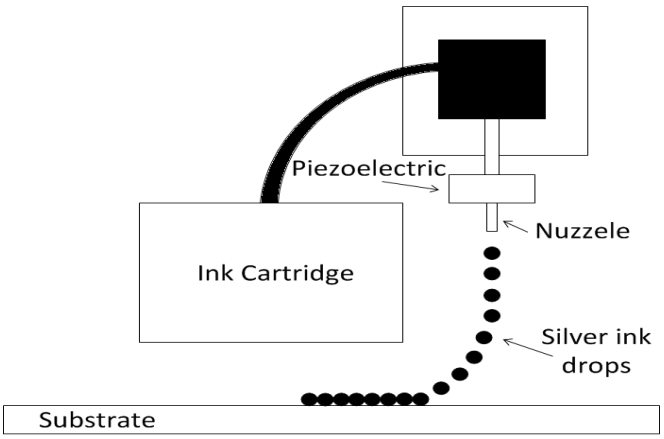

Figure 4.1. Schematic of a piezoelectric DOD inkjet-printer.

The platen which holds the substrate and the print head can be moved with electric precision motors hence the pattern can be printed. The volume of the droplet is depends on the volume of the print head which is commercially varies between 500 fL to 2 nL. The diameter of the printed droplets depends on ink viscosity, ink temperature, jetting

voltage, the pulse shape and frequency, and properties and temperature of the substrate [14]. For both dielectric and conductor inks it is essential to cure or sinter them after printing. Conductive inks are made of metallic nanoparticles or conductive polymers which are bonded together in order to form solid and uniform layer of metal in the sintering procedure. The temperature and time in the sintering process have significant effect on the conductivity of the printed traces. Figure 4.2 depicts the difference of a conductor printed pattern before and after sintering. Typically the metallic parts used in conductor inks are silver, gold or copper nanoparticles with 2 to 4 times higher resistivity than their pure counterparts. Among these different inks silver ink is more popular since it has the highest conductivity and being anti-oxidation. [14]

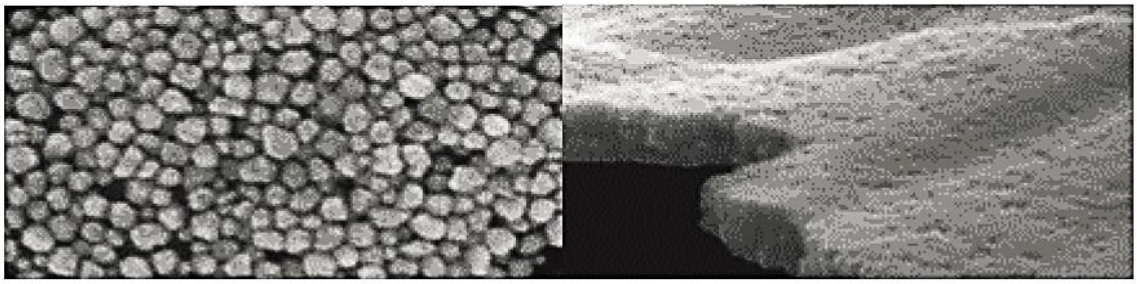

(a) (b)

Figure 4.2. The effect of sintering on conductive ink: (a) before sintering and (b) after sintering at 180℃ for 10 minutes. [14]

The utilized printer in this project is a Fujifilm Dimatix DMP-2831 material inkjet printer shown in Figure 4.3 with the platen area of 210 mm× 310 mm. The temperature of the platen and the cartridge can be controlled by 1℃ precision within 40 ℃ to 60 ℃ for the platen and 28 ℃ to 35 ℃ for the cartridge. Each cartridge has 16 nuzzles with 254 µm spacing in a single row, the volume of the droplets are 10 pL and the pulse voltage can be assigned between 18 V and 35 V. The resolution of the printed patterns can be specified from 100 dot-per-inch (dpi) to 5080 dpi depends on the droplet size on the substrate.

Figure 4.3. (a) Dimatix DMP 2831 material inkjet printer. (b) The cartridge and head used for printing.

5. CHARACTERIZATION OF THE SUBSTRATE AND CONDUCTOR INK

In this project silver ink is utilized as the conductor ink because of the higher conductivity of silver ink compared to copper and gold inks, affordable price compared to gold ink, and being anti-oxidation compared to copper ink. As an organic substrate, paper has the potential for the realization of environmentally-friendly and recyclable electronics [1]. Because of being ultra-low-cost and compatible with printing it is tempting to use paper as a substrate for implementation of electronic circuits [3]. As it was discussed before, inkjet-printing features the possibility to enhance the production versatility. It is also suitable to print electronic circuits on unconventional substrates such as wood, ceramic and paper.

Since there is no investigation about the electrical properties of a low-cost fibrous substrate like cardboard, these properties should be characterized in the first step. In addition, the electrical features of the printed conductive ink on cardboard should be investigated in order to enable the effective implementation of efficient microwave structure [16].

5.1 Characterization of Cardboard

In this project Stora Enso packaging thin cardboard is exploited as the substrate. In order to design the passive microwave circuits such as antennas or filters it is essential to have the permittivity and loss tangent of the substrate. There are different ways to characterize the RF/Microwave properties of a substrate like split-cylinder resonator, ring resonator, high-quality (high Q) structures and two transmission-line methods [17]. The resonator based methods have the advantages of simple realization and utilization for extraction of permittivity while the obtained values are only at the resonance frequencies and the dispersion of resonator on the substrate appears at higher frequencies. On the other hand transmission line based methods are simple in implementation while de-embedding and through-reflection-line (TRL) calibration is needed in order to remove the effect of connectors in the measurement [17]. One of the most accurate methods is the two transmission-line methods in which two identical transmission lines with different lengths are fabricated on the same substrate. Using the phase difference of the signals the effective permittivity of the substrate can be obtained. Whereas by comparing the magnitude of insertion losses of two lines the value of the loss tangent can be extracted [16]. In this method there is no need to de-embed or use TRL calibration because all the calculations are based on transmission-line length difference. The geometry of the two-transmission-line method is depicted in Figure 5.1.

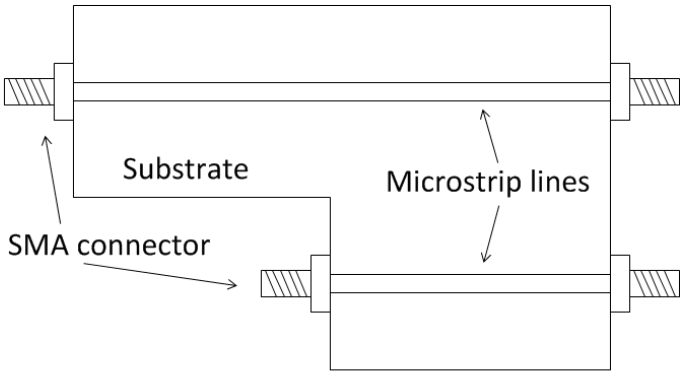

Figure 5.1. The geometry of two-transmission-line method.

The effective permittivity of the substrate can be obtained by measuring the phase difference of the output signals in the lines. Equation (5.1) shows the relationship of the effective permittivity and the phase difference.

$$\varepsilon_{eff} = (\frac{\Delta\theta \times C}{2\pi f \times \Delta L})^2, \quad (5.1)$$

where, C is the speed of light, $\Delta\theta$ is the phase difference of the output signals, f is the frequency, and ΔL is the length difference of the lines. In a general lossy transmission-line the magnitude of the output power P_{out} can be determined by knowing the magnitude of the input power P_{in} and propagation loss α.

$$|P_{out}| = e^{-2\alpha l}|P_{in}|, \quad (5.2)$$

where

$$P_{out} = \frac{{V_{out}}^2}{Z_0}, \quad (5.3)$$

$$P_{in} = \frac{{V_{in}}^2}{Z_0}, \quad (5.4)$$

l is the length of the transmission-line, V_{in} is the input voltage, V_{out} is the output voltage and Z_0 is the characteristic impedance of the line [10]. In addition, since the measurements are usually done based on S-parameters the aforementioned equations can be re-written as

$$S_{21} = \frac{\frac{V_{out}}{Z_0}}{\frac{V_{in}}{Z_0}} = \frac{V_{out}}{V_{in}}. \quad (5.5)$$

Thus,

$$|S_{21}|^2 = \frac{|P_{out}|}{|P_{in}|} = e^{-2\alpha l}. \quad (5.6)$$

Therefore, by measuring S_{21} for a transmission-line and by knowing the accurate length it is feasible to find the propagation loss in the line using equation (5.6). As it

was discussed before the two-transmission-line technique is utilized to get read of the effect of connectors and junctions. In this case, equation (5.6) can be rewritten as

$$\frac{|S_{21}{}^{long}|}{|S_{21}{}^{short}|} = \frac{e^{-\alpha l_{long}}}{e^{-\alpha l_{short}}} = e^{-\alpha(l_{long}-l_{short})} = e^{-\alpha \Delta l}, \quad (5.7)$$

where l_{long} is the length of the longer line, l_{short} is the length of the shorter line and Δl is the length difference of the two lines. Hence, by measuring S_{21} of two identical transmission lines with different lengths it is feasible to find the propagations loss consists of conductor loss α_c, dielectric loss α_d, and radiation loss α_{rad} [10]. For the microstrip transmission line much shorter than 10 times wavelength the radiation loss is negligible. If the properties of the conductor are known, the dielectric loss can be extracted. Usually, the dielectric loss is represented using loss tangent which is expressed using equation (5.8)

$$tan\delta = \frac{\omega\varepsilon'' + \sigma}{\omega\varepsilon'}, \quad (5.8)$$

where ω is the angular frequency, ε'' is the imaginary part of permittivity, σ is the conductivity of substrate, and ε' is the real part of permittivity of substrate [10]. After extracting the dielectric loss, using equation (5.9) the loss tangent can be calculated.

$$tan\delta = \frac{2\alpha_d\sqrt{\varepsilon_{eff}}(\varepsilon_r - 1)}{f\beta\varepsilon_r(\varepsilon_{eff} - 1)}, \quad (5.9)$$

In order to obtain the conductor loss, the properties of conductor such as conductivity, surface resistance, width and thickness should be known. Conductor loss can be acquired utilizing equation (5.10).

$$\alpha_c = \frac{\sqrt{\omega\mu/2\sigma}}{Z_0 W} \quad (5.10)$$

Since for the characterization of the substrate, the conductor properties should be known, copper tape is utilized in order to implement the microstrip lines and ground planes. The conductivity, thickness and width of the copper microstrip lines implemented on cardboard are 5.8×10^7 S/m, 50 µm and 2 mm, respectively. Three identical microstrip lines are implemented with different lengths which are 5 mm, 10 mm and 15 mm to compare the results two by two and have more accurate results compared to the case in which only two lines are utilized. The fabricated samples are illustrated in Figure 5.2. The thickness of the cardboard is 560 µm and it was maintained in an ordinary oven with air circulation at 150 ℃ for 1 hour since for inkjet-printed circuit the same condition is utilized for sintering the silver ink.

Figure 5.2. The fabricated microstrip lines on sintered cardboard.

The magnitude and phase of S_{21} are measured with an Agilent PNA E8358A two port vector network analyzer (VNA) between 500 MHz and 3 GHz after full two port short_open_load_thru (SOLT) calibration. Then, using equations (2.40) and (5.1) the relative permittivity of substrate is calculated. For loss tangent using equation (5.7) the total propagation loss of the line is calculated, using equation (5.10) conductor loss is obtained. Finally, utilizing equation (5.9) loss tangent can be calculated. The same parameters can be measured using Agilent 85070 Dielectric Probe Kit in the same frequency interval. The measurement results for the relative permittivity and loss tangent of cardboard obtained using the two-transmission-line method and Dielectric Probe are depicted in Figure 5.3 and Figure 5.4.

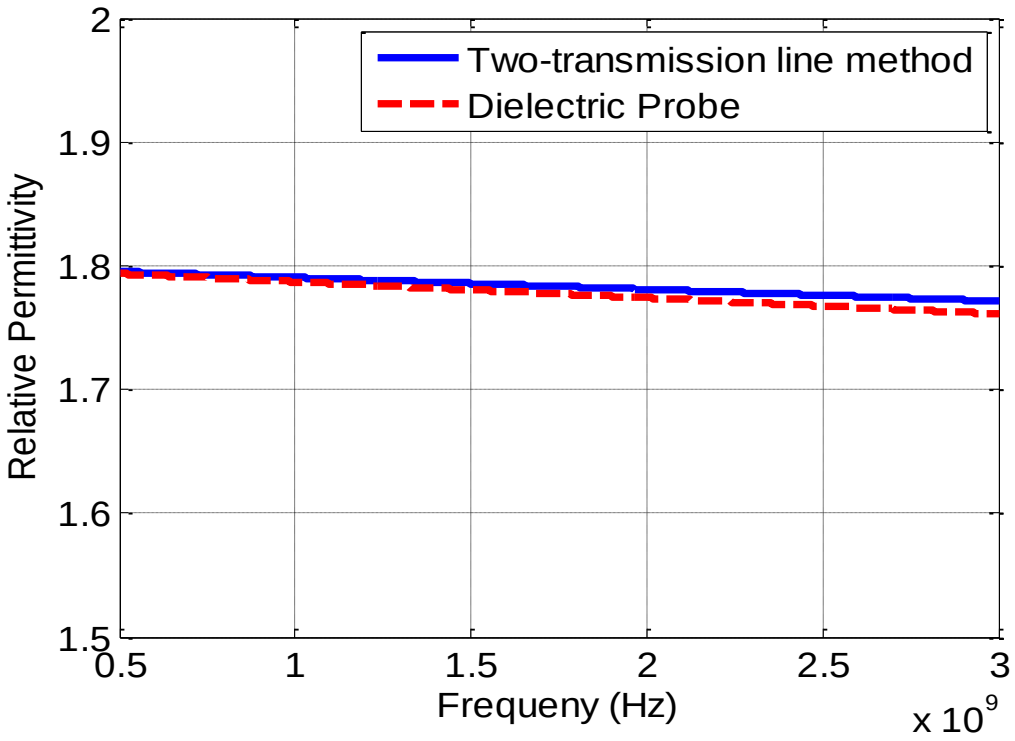

Figure 5.3. The measurement results for the relative permittivity of cardboard using two-transmission-line method and dielectric probe.

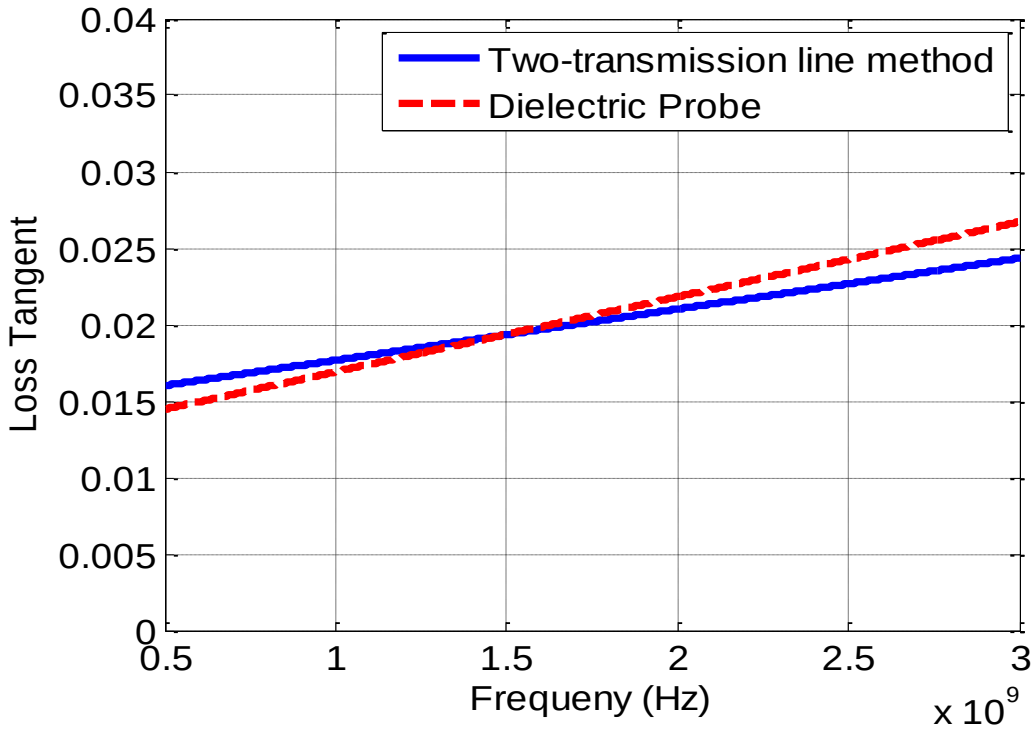

Figure 5.4. The measurement results for the loss tangent of cardboard using two-transmission-line method and dielectric probe.

5.2 Characterization of the Printed Silver Ink

In this project NPS-JL silver ink with 55.5wt% metal content is used to print the conductor traces. In order to characterize the electrical properties of the printed silver trace, the two-transmission-line method is utilized while the properties of the substrate are known in this case. For this purpose appropriate printing procedure should be applied to maximize the conductivity of printed traces. For the first step, the appropriate resolution for the printed pattern should be obtained. In order to have both suitable connection between the droplets and to avoid the droplets spread on the substrate, the most suitable spacing between the droplets is equal to the radius of droplets on the substrate. The radius of the droplets and their pattern depend on the properties of ink and substrate such as, viscosity, contact angle, temperature, hydrophilicity and roughness. There is a possibility to measure the droplet radius utilizing the printer in a specific manner which is called droplet test. The measurement results of the droplet size on both sides of cardboard are illustrated in Figure 5.5. As can be seen the diameter of droplets are almost in the range of 80 µm to 90 µm. Accordingly, the appropriate resolution for the printing is 635 dpi for both sides of the substrate.

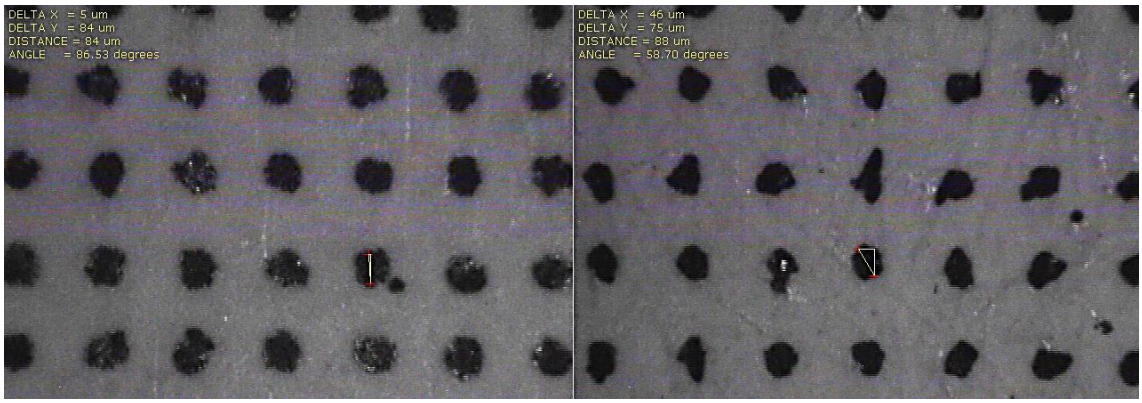

Figure 5.5. The drop test results on both sides of the utilized cardboard.

In order to have better conductivity it is needed to print more layers of silver ink but the problem is that when the number of printed layers in one turn is high the achieved conductivity is lower than expectation due to the time which is needed for printing more layers. The conductivity of silver ink is higher when it is sintered more quickly. In addition, if the layers are printed separately then the total printing and sintering time is increased dramatically since at least one hour is essential to sinter each layer. Therefore, there is a trade-off between the number of printed layers and the time needed for fabrication of the whole circuit. In order to find the basic idea of how print the circuit from the number of layers point of view, a simple test can be done by measuring the DC resistance of the different printed trances. For this purpose three scenarios are defined while in the first scenario the layers are printed and sintered separately, in the second scenario each two layers are printed and sintered in one turn, and in the last scenario each three layers are printed and sintered in one turn. After sintering the DC resistances of the rectangular 2mm × 20mm patterns are compared and expressed in Table 1.

Table 1. The DC resistance of the printed silver trace on cardboard in different scenarios.

Number of printed layers in each turn	First turn	Second turn	Third turn	Fourth turn	Fifth Turn	Sixth turn	Seventh turn
1 layer	∞	3.26 Ω	2.3 Ω	1.6 Ω	1.45 Ω	1.38 Ω	1.33 Ω
2 layers	∞	2.06 Ω	1.51 Ω	1.39 Ω	-	-	-
3 layers	∞	2.38Ω	1.47 Ω	-	-	-	-
Required sintering time	1 h	2 h	3 h	4 h	5 h	6 h	7 h

By comparing the resistance of the lines and the fabrication time, it can be deduced that printing and sintering 2 layers in one turn and printing 8 layers in total is the suitable choice from both the conductivity and required time points of view. Therefore, this procedure is utilized to fabricated microstrip lines in order to determine the conductivity of printed silver traces. Figure 5.6 depicts the fabricated transmission lines on cardboard using silver ink.

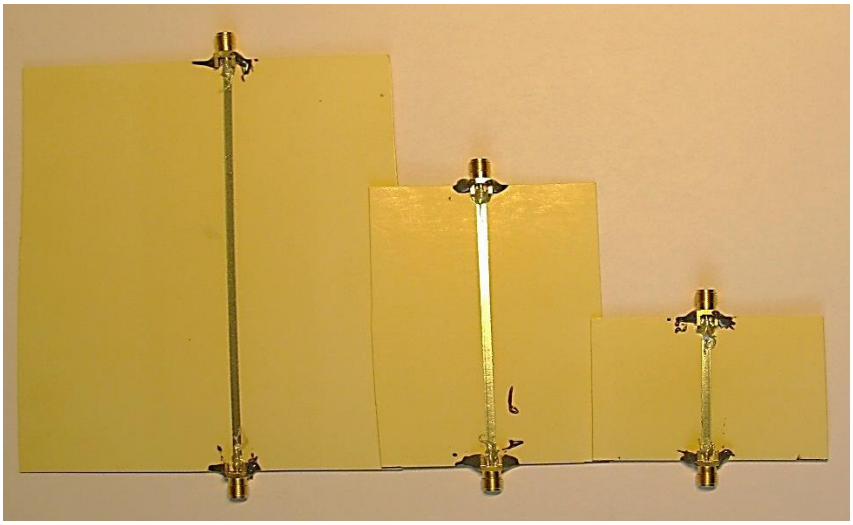

Figure 5.6. The fabricated microstrip lines on cardboard using silver ink in order to find the conductivity of the printed silver traces.

The obtained value for the conductivity of the printed silver traces in this case is 1×10^{7} S/m. The thickness of the conductor is an important parameter which affects the high frequency losses of the whole circuit. The investigation on the thickness of the printed silver traces shows that the ink is penetrated into the substrate due to being fibrous. This penetration is approximately 45 μm which reduces the conductivity dramatically since the high temperature essential for sintering cannot reach into the substrate. Moreover, if the ink penetrates into the fibers of the substrate the conductivity decreases

because it is partially conductor and the rest is the paper which is not conductive. Thus, it is necessary to coat the substrate surface with a thin layer of ink-proof dielectric material. In addition, it is beneficial if this material enhance the roughness of the surface because having high values of roughness increases the high frequency losses. For this purpose a conventional primer composed of tetrahydrofurfuryl acrylate, ethoxylated trimethylolpropane triacrylate, 2-hydroxy-2-methyl-1-phenyl-propan-1-one, and bis-phenylphosphineoxide is utilized in the rough and fibrous side of cardboard since the other side has better situation [18]. In order to have appropriate smooth ink-proof surface 5 layers of primer in ink form is printed with 1016 dpi resolution on the rough surface of cardboard and cured separately in 5 turns. In each turn after printing, the sampled is cured with ultra-violet (UV) light for 10 minutes then maintained at 150 ℃ for 1 hour in the oven. UV light is utilized to cure the printed primer while oven is used to evaporate the water content inside primer ink and avoid the later reaction between primer and silver ink. The cross section of the printed silver traces on cardboard before and after treatment is illustrated in Figure 5.7. The cardboard surface roughness, before and after treatment using primer is measured with an optical profilometer. Using the measured values for the roughness it can be deduced that the peak-to-valley distance before and after treatment are 39 µm and 11.5 µm, respectively on the rough side. In addition, the mean roughness and root mean squared roughness are 1.68 µm and 2.13 µm before treatment, respectively and enhanced to 1.3 µm and 1.62 µm after surface treatment using primer. The roughness situation on the other side of the cardboard is much better and treatment is not needed since the peak-to-valley distance, mean roughness and root mean squared are 19 µm, 1.22 µm and 1 µm, respectively. The results for the roughness of rough side of the cardboard before and after treatment and smooth side of cardboard are represented in Figure 5.8.

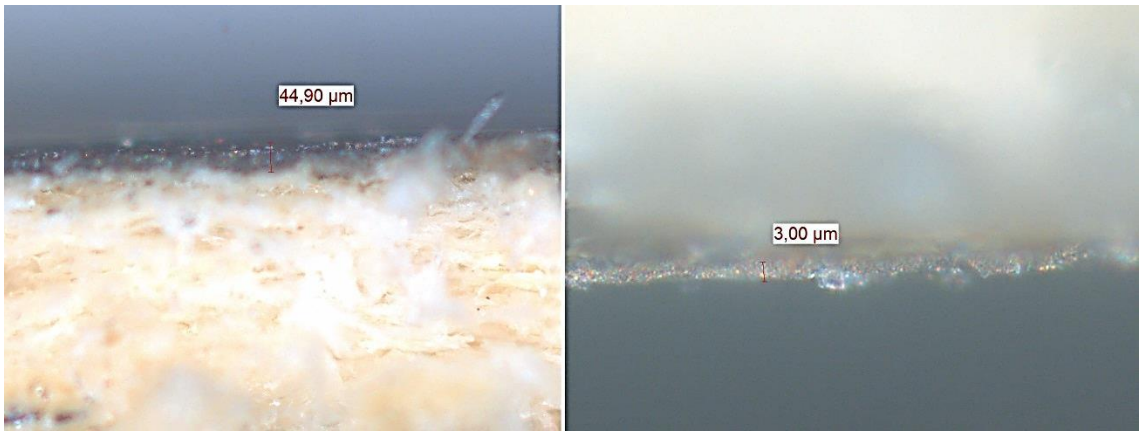

(a) (b)

Figure 5.7. (a) The silver ink penetration into the substrate before treatment with 5x magnification. (b) The thickness of silver ink on primer after treatment with 20x magnification.

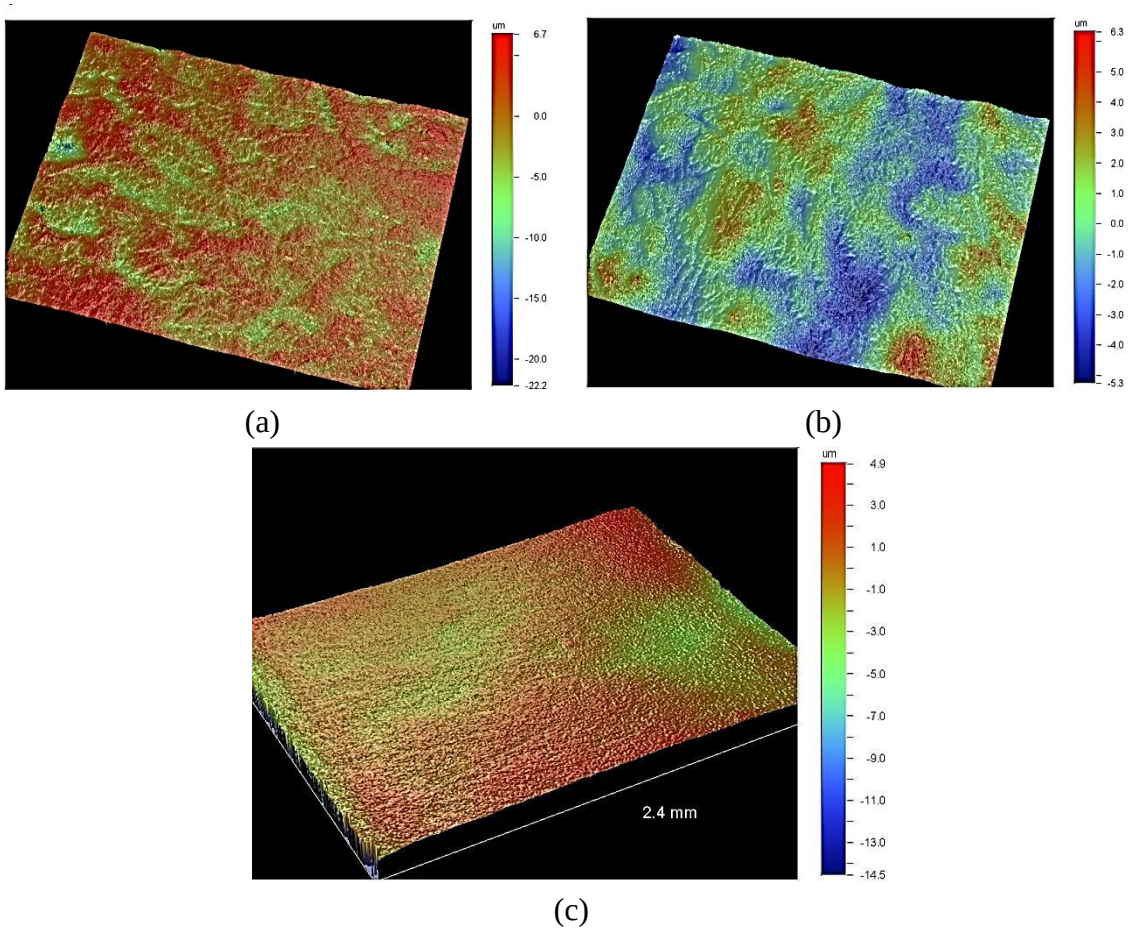

Figure 5.8. The measurement results for the roughness of the surface. (a) Rough side before treatment. (b) Rough side after treatment. (c) Smooth side.

In order to determine the conductivity of the printed silver traces after the surface treatment three microstrip lines with the aforementioned physical dimensions are implemented and the obtained value in this case is 2×10^7 S/m. All the essential properties of the substrate and conductor required for design and simulation are obtained and represented in Table 2.

Table 2. The measured parameters for cardboard and silver ink.

Measured Parameters	Value
Relative permittivity of cardboard	1.78
Loss tangent of cardboard	0.025
Thickness of cardboard	560 µm
Conductivity of silver ink	2×10^7 S/m
Thickness of silver ink	3 µm

5.3 Implementation of RF Circuits

In this section two basic RF structures are designed and simulated utilizing the obtained values for the substrate and conductor, and then the discrepancies between the simula-

tion and measurement are investigated in order to assess the accuracy of the model. For this purpose a band stop filter and a patch antenna for 2.45 GHz are designed and simulated. The simulations are done using the 3D full wave electromagnetic simulator Ansys HFSS based on finite element method.

5.3.1 Band Stop Filter

The band stop filter consists of a 50 Ω microstrip line and a quarter-wavelength open stub which acts as a short circuit at 2.45 GHz and avoids the signal to pass through the transmission line. Equations (5.11) and (5.12) are used in order to design the band stop filter [10]. The geometry of the proposed band stop filter with physical dimensions, the fabricated filter on cardboard and comparison between the simulation and measurement values are depicted in Figure 5.9 and Figure 5.10, respectively. As can be seen in these figures the simulation and experimental results are in a good agreement with each other.

$$W = h \times \frac{2}{\pi}\left[\frac{377\pi}{2Z_0\sqrt{\varepsilon_r}} - 1 - \ln\left(2 \times \frac{377\pi}{2Z_0\sqrt{\varepsilon_r}} - 1\right) + \frac{\varepsilon_r - 1}{2\varepsilon_r}\left\{\ln\left(\frac{377\pi}{2Z_0\sqrt{\varepsilon_r}} - 1\right) + 0.39 - \frac{0.61}{\varepsilon_r}\right\}\right] = 2mm \quad (5.11)$$

$$L_{stub} = \frac{\lambda}{4} = \frac{c}{4f\sqrt{\varepsilon_r}} = 23\ mm \quad (5.12)$$

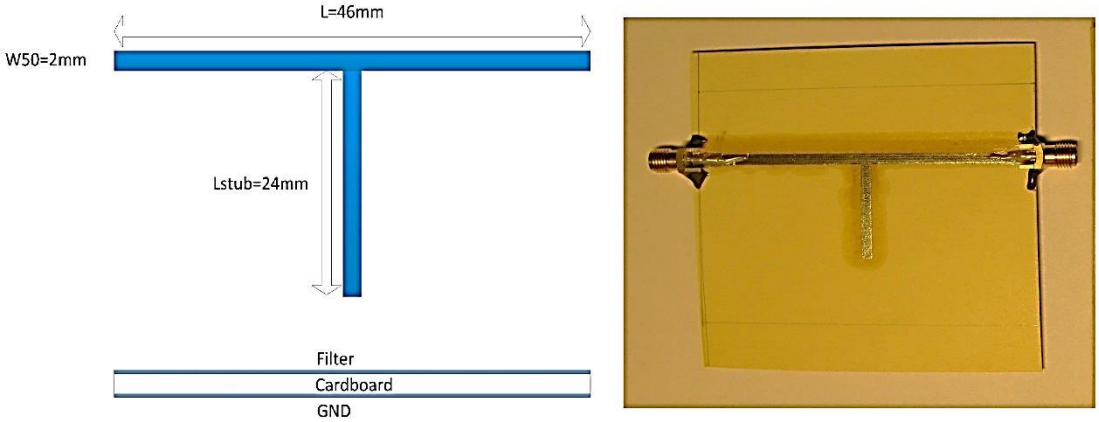

(a) (b)

Figure 5.9. (a) The geometry of the proposed band stop filter with physical dimensions. (b) The fabricated filter on cardboard using silver ink.

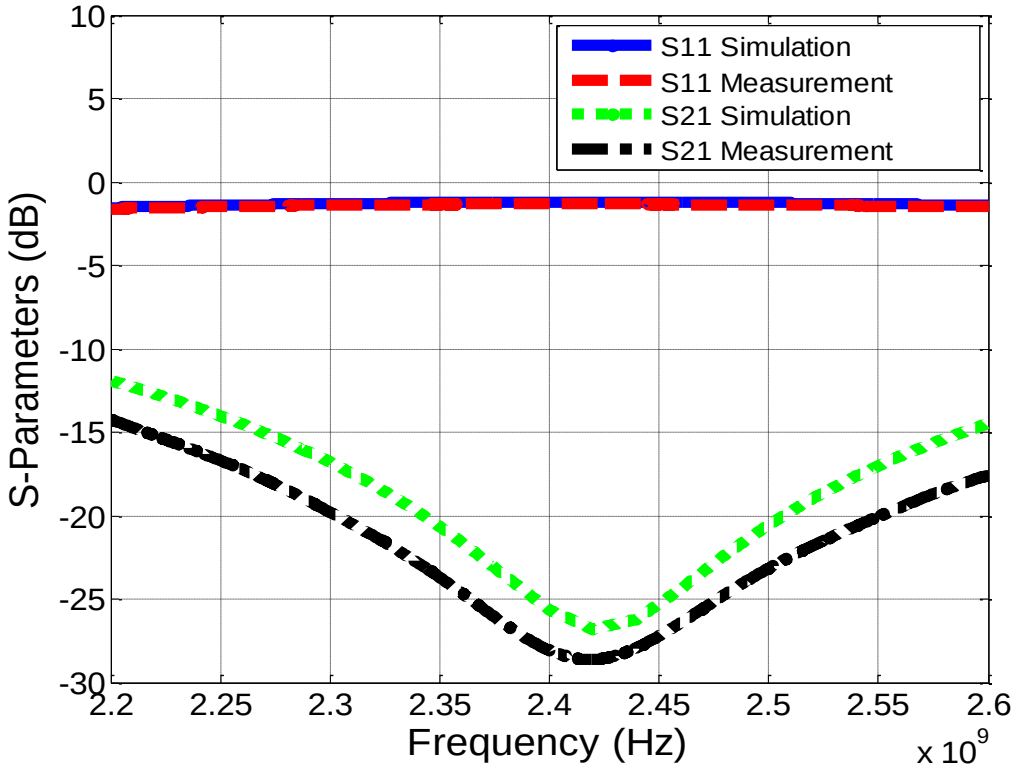

Figure 5.10. The simulation and experimental results for S-parameters of the band stop filter.

5.3.2 Patch Antenna

A patch antenna consists of the radiating patch, signal feeding, ground plane and substrate. In order to design a patch antenna for 2.45 GHz, using equations (5.13) to (5.15) the physical dimensions should be calculated [12]. In order to have appropriate matching, inset feeding is chosen which is implementable with inkjet-printing. The patch antenna is designed such that the dominant resonant frequency is TM_{010} excitation mode. The geometry and fabricated patch antenna with physical dimensions are depicted in Figure 5.11.

$$W = \frac{C}{2f_r\sqrt{\varepsilon_r}} = 46\ mm \qquad (5.13)$$

$$y_i = \frac{W}{\pi}\cos^{-1}\sqrt{\frac{50}{R_{in}}} = 7.5\ mm \qquad (5.14)$$

$$R_{in} = \frac{1}{2(\frac{1}{90}(\frac{W}{\lambda_0})^2)} = 320\ \Omega \qquad (5.15)$$

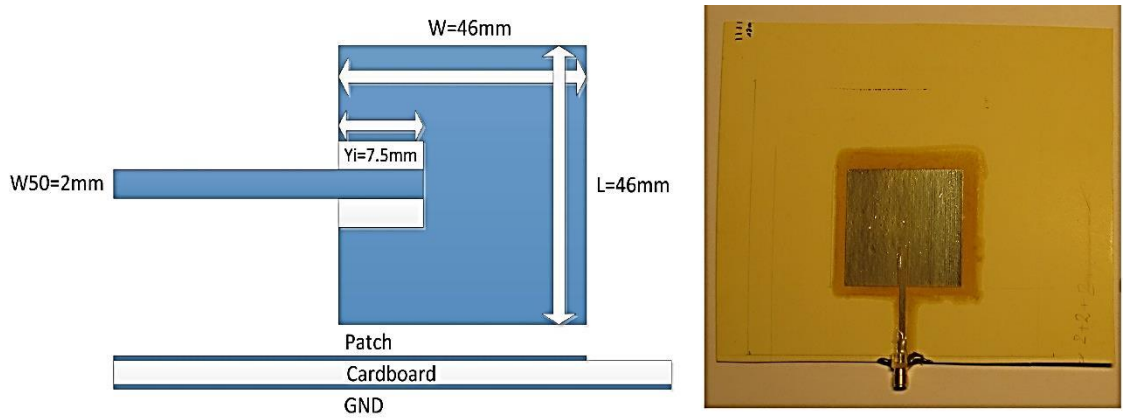

Figure 5.11. The geometry and fabricated patch antenna.

The simulation and measurement results for return loss, realized gain and radiation efficiency of the patch antenna are illustrated in Figure 5.12. For measuring the efficiency and gain of the antenna near-field measurement device Satimo Starlab, and for the return loss an Agilent PNA E8358A two port VNA are utilized.

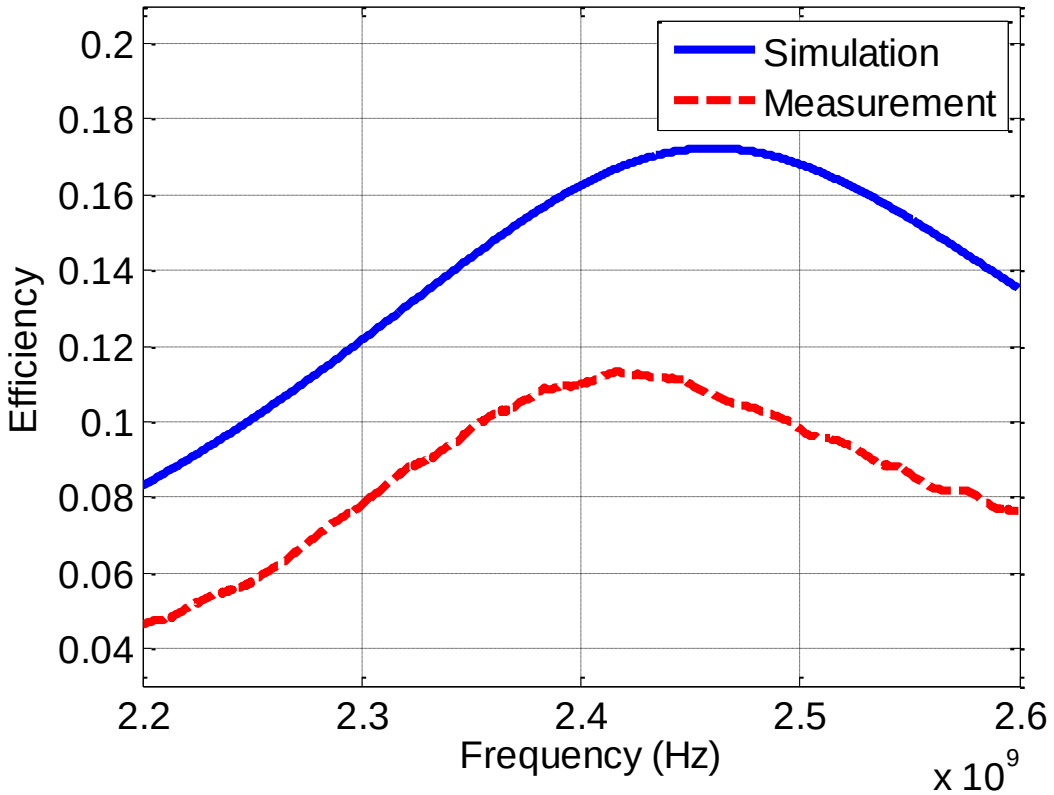

(a)

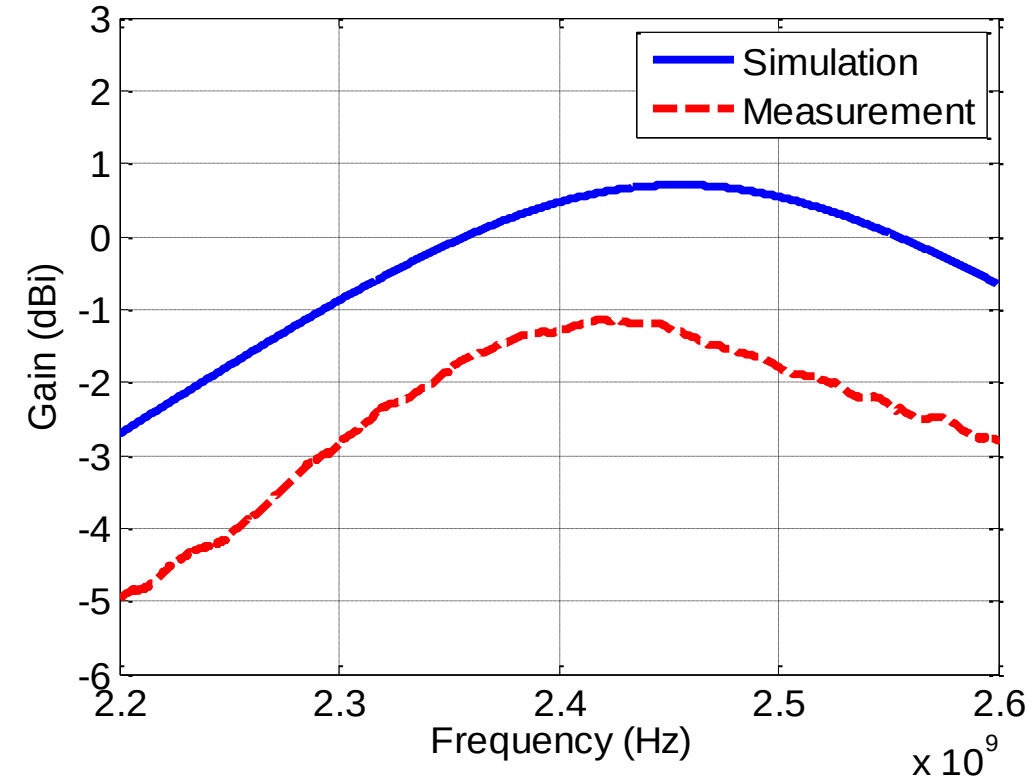

(b)

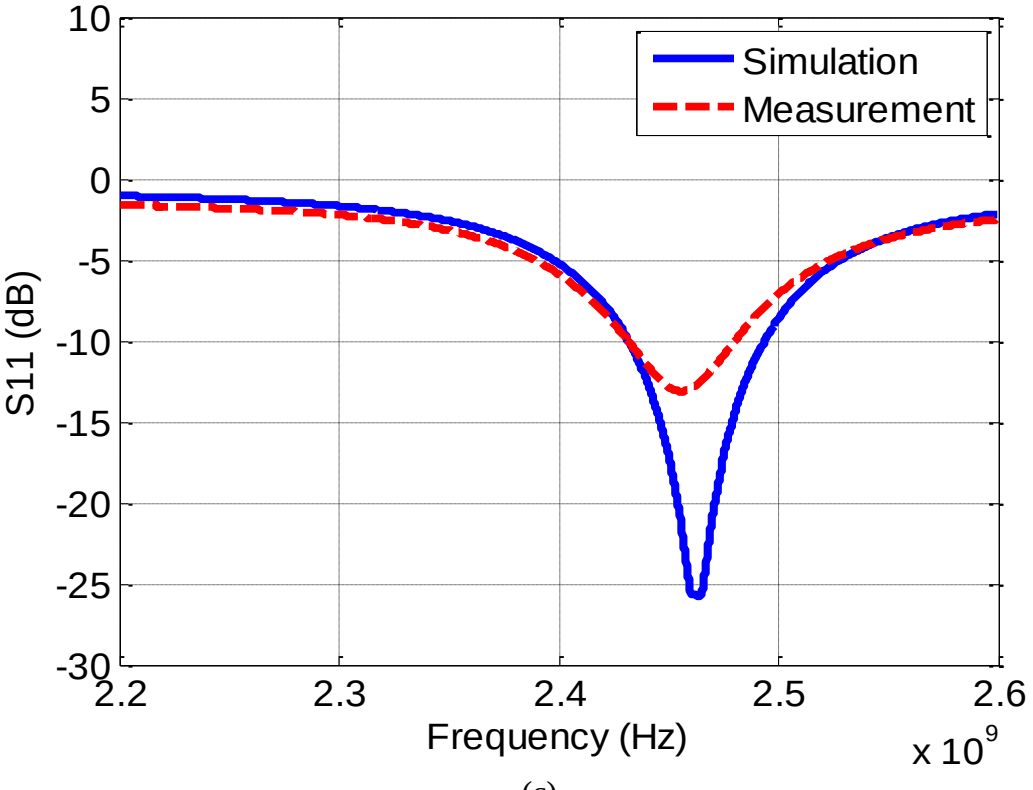

(c)

Figure 5.12. The simulation and measurement results of the inkjet-printed patch antenna on cardboard for (a) the radiation efficiency, (b) maximum realized gain and (c) return loss.

As can be seen there is a slight difference between the simulation and experimental results. There are two potential reasons for this phenomenon; the first one is the misalignment of different printed layers because of the inaccuracy of the printer (± 25 µm) and users mistakes, and the other one is the inaccuracy of the measurement equipment (±0.7 dB for the peak gain at 1880 MHz). Regarding to the first issue the misalignment of printed layers is measured using an optical microscope and approximately 130 µm distance is observed. Since this phenomenon increases the losses at the radiating edges of the patch antenna and of the feeding line, it is expected that by including it in the simulation model, the results should be more similar to the measurement. Figure 5.13 shows that the maximum magnitude of the current distribution occurs in the regions where the misalignment has happened. In addition, due to the lower thickness of the printed layers on the edges compared to the rest of structure the losses are higher. Hence, the efficiency and gain of the patch antenna degrades. The comparison between the simulation and measurement results of the new simulation model are represented in Figure 5.15. It can be deduced that the matching between the simulated and measured efficiency and gain improved by 1.5 % and 1 dB, respectively.

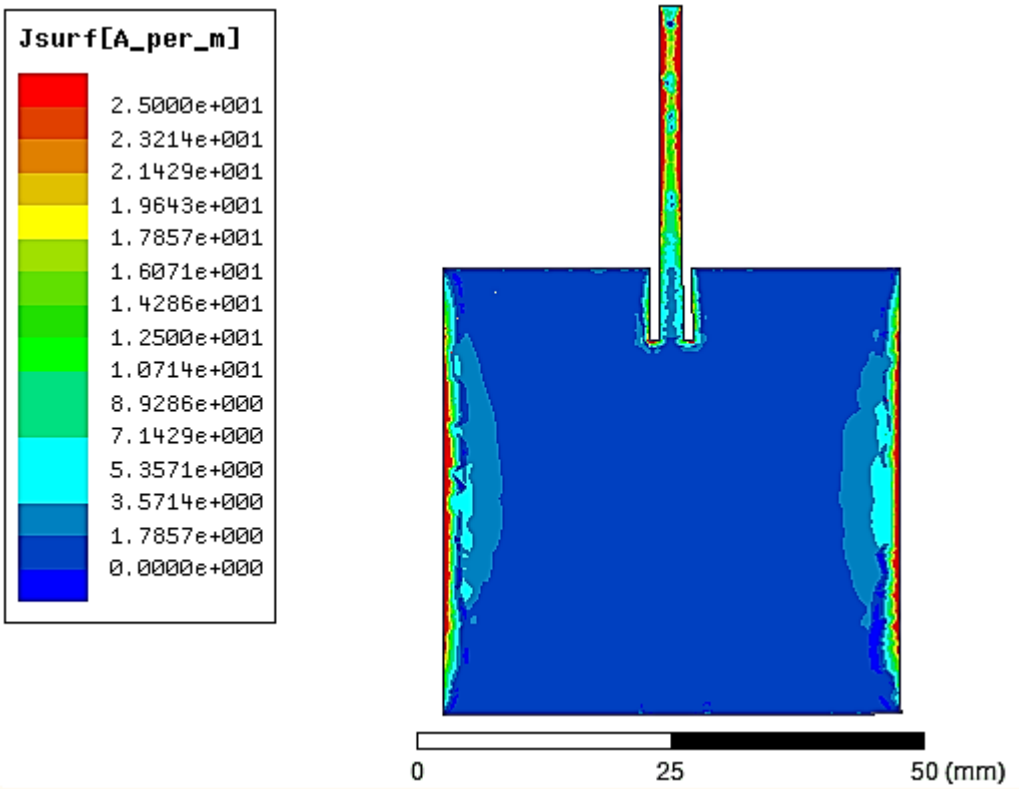

Figure 5.13. The current distribution of the patch antenna at 2.45 GHz.

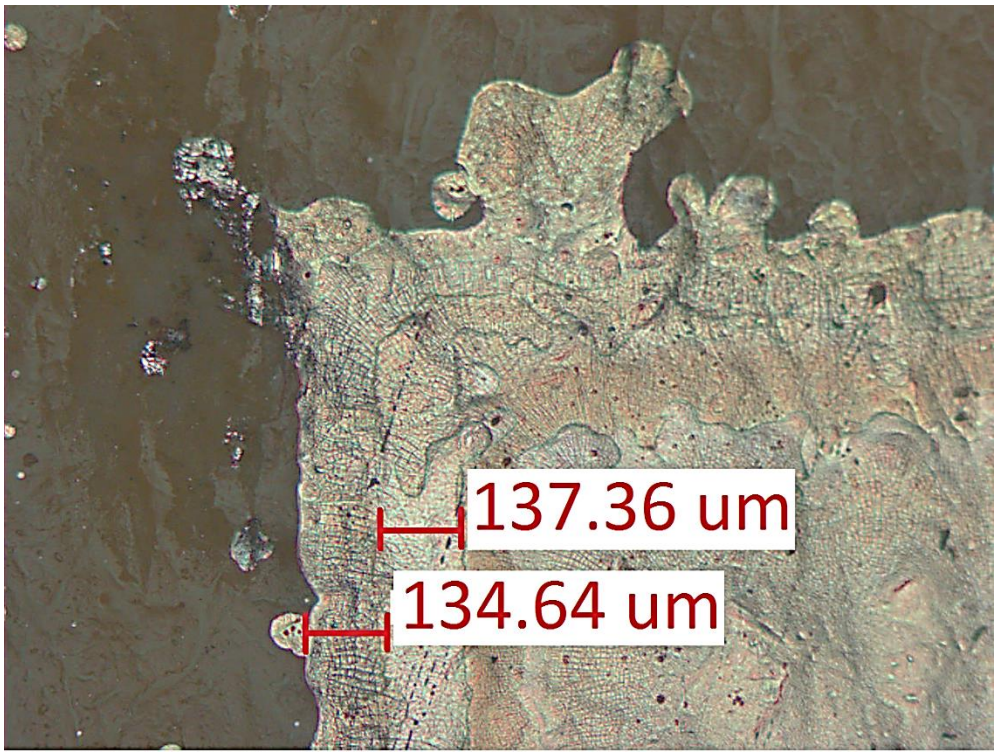

Figure 5.14. The misalignment of the printed silver traces on cardboard 5x magnification.

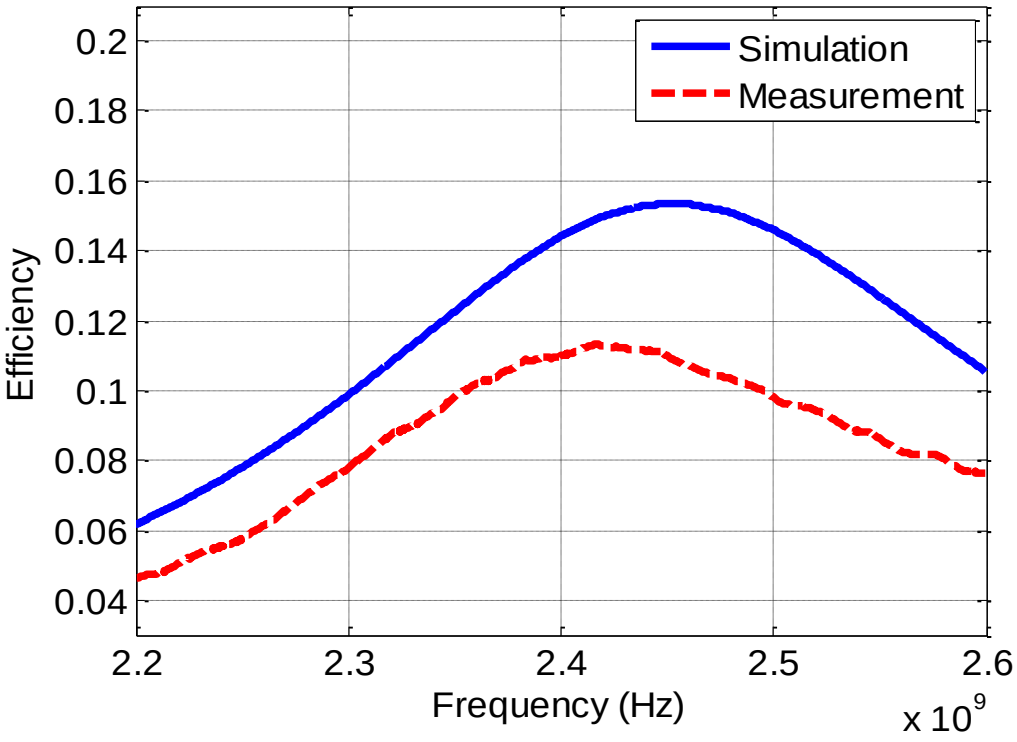

(a)

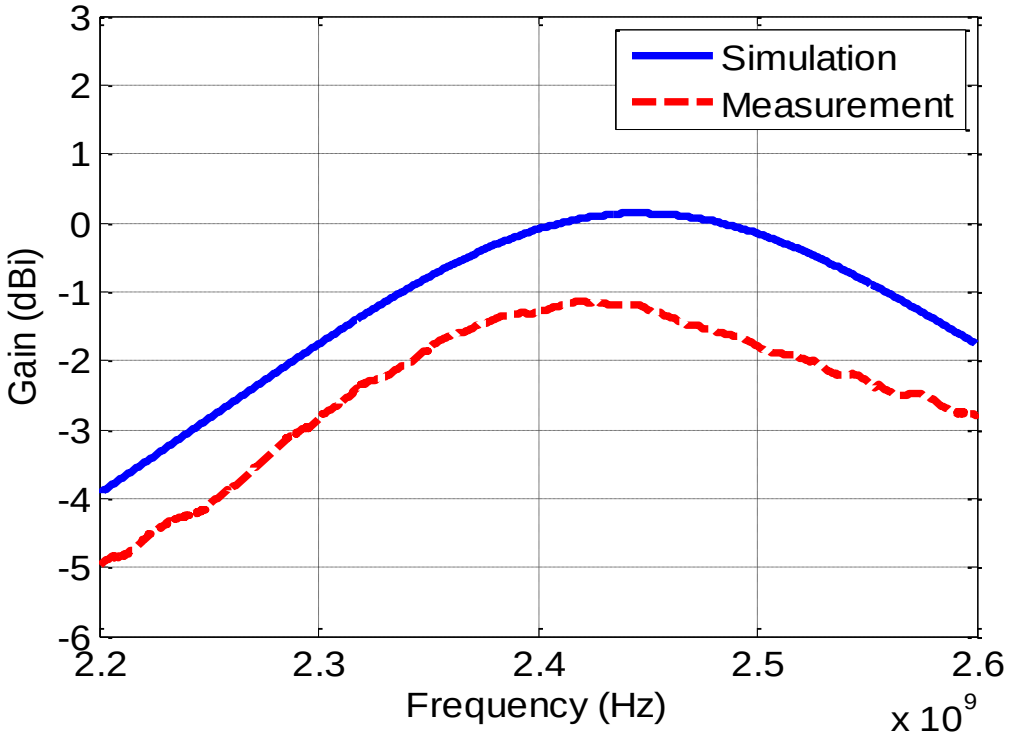

(b)

Figure 5.15. The simulation and measurement of the patch antenna considering the layers misalignment for (a) the radiation efficiency and (b) maximum realized gain.

The simulation and experimental results for normalized radiation patterns of the inkjet printed patch antenna using the obtained model is illustrated in Figure 5.16.

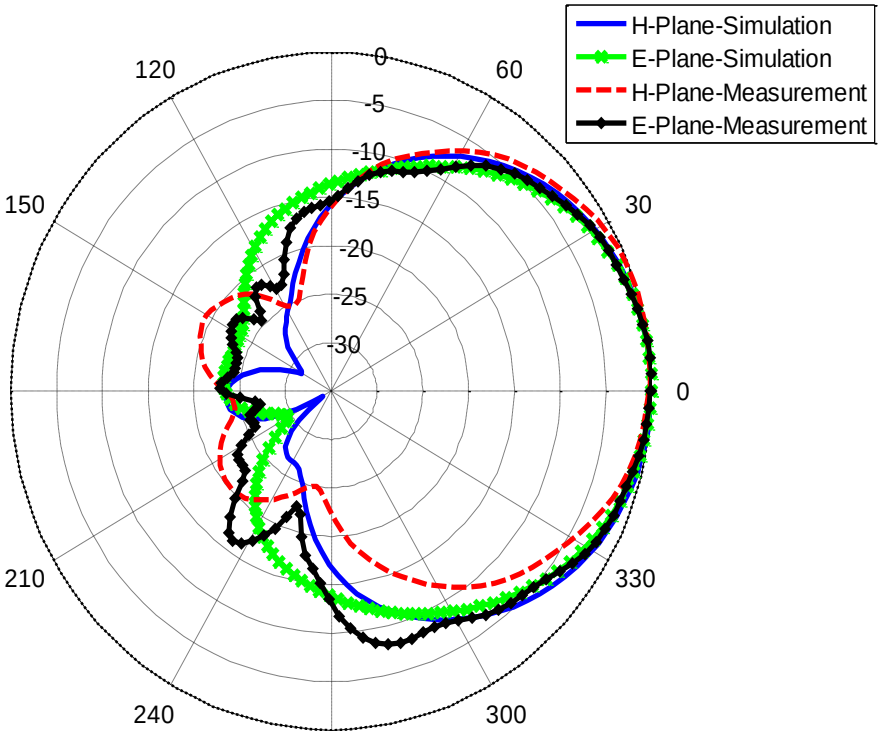

Figure 5.16. The simulation and measurement results for the radiation patterns of the inkjet-printed patch antenna.

6. WIDE BAND ANTENNA

The environment we are living in is full of transmitted electromagnetic signals for radio and television broadcasting and communication. Most of these signals are propagated in the medium and absorbed by the receivers or dissipated. Thus, if the useless part of the transmitted signals is harvested by a device it is feasible to fabricate the battery-less circuits which are appropriate for environmentally-friendly applications. Usually a power-harvester circuit consists of an antenna, rectifier, voltage booster, regulator and energy reservoir. In this chapter a wide-band inkjet-printed antenna is designed and fabricated on cardboard utilizing silver ink for power-harvesting application. For the power harvester part a P2110 powerharvester module is utilized. P2110 has rectifier, voltage booster and regulator and management system inside the module so only an antenna as the input of the circuit and an ultra-capacitor as the energy reservoir should be connected to the module. According to its datasheet, the circuit has a wide bandwidth between 600 MHz and 1.5 GHz. Thus, -10 dB bandwidth of the desired antenna is assumed the same. For the other specification it is better to have an omnidirectional pattern in order to have the possibility to absorb the radiated power from all directions. In this chapter the design procedure of a monopole planar wideband antenna is investigated, then fabricated using inkjet-printing technology on cardboard and finally the measurement results are compared with the simulations.

6.1 Theory of Planar Wide Band Antenna

Since using inkjet-printing planar antennas can be implemented, among different categories of broadband antennas microstrip type is the most appropriate choice. In addition, the antenna port should be unbalanced because the input of the power harvester module is also unbalance. The input impedance of the antenna should be 50 Ω due to the fact that the whole system is in 50 Ω impedance. There are some techniques that can increase the bandwidth of a conventional microstrip patch antenna such as increasing the thickness of the substrate or decreasing its permittivity but it is not possible to achieve more than 10% bandwidth to central frequency ratio [19]. While, for the desired application this ratio should be in the range of 100% or in other words the ratio of the lower to higher cut-off frequency should be 1:3. By these specifications the available options are planar multiresonator broadband microstrip antennas, multilayer broadband microstrip antennas, stacked multiresonator microstrip antennas, and broadband planar monopole antennas [19].

6.1.1 Planar Multiresonator Broadband Microstrip Antennas

In this method a single patch antenna is fed and the other patches are coupled to the main patch by using either a narrow gap or thin microstrip line. Different types of patch shape like rectangular, circular and triangular can be utilized in order to make multi-resonator antennas. The achievable bandwidth for this type is in the range of 5% to 20% which is much lower than the desired value [20], [21]. In addition, the total size of the antenna is large and the radiation pattern varies with respect to the frequency which are not suitable for the desired application [19].

6.1.2 Multilayer Braodband Microstrip Antennas

In this method similar to the previous one multiple resonators are used but instead of being in the same plane they are stacked in different layers. The overall size of the antenna does not increase by exploiting this method but the thickness increases [19]. It is feasible to achieve up to 70% bandwidth with this method with a small variation of the radiation pattern with respect to the frequency [21], [22]. But the implementation of the antenna on cardboard using this method is complicated since it is hard to stack different layers of cardboard and the appropriate facilities are needed [3].

6.1.3 Stacked Multiresonator Microstrip Antennas

Stacked multiresonator microstrip antennas can be implemented if the multiresonator microstrip antennas are stacked in different thick low permittivity layers. In other words this technique is the combination of the two latest methods [19]. Alike the multilayer antennas it is not practical to stack layers of cardboard. Moreover, the obtained radiation pattern is not omnidirectional [19].

6.1.4 Broadband Planar Monopole Antennas

A monopole antenna consists of the radiating branch and the ground plane, is one of the basics antennas geometry. The first resonance of monopole antenna occurs when the length of the radiating branch is quarter wavelength [12]. A monopole antenna can be described as a dipole antenna which is divided in half and fed against a ground plane [13]. The geometry of a general monopole antenna is illustrated in Figure 6.1. The radiating branch is perpendicular to the ground plane which in the ideal case the size of the ground plane is infinite. A planar monopole antenna is a monopole antenna that both the radiating branch and ground planes are in parallel planes. There are various types of planar monopole antennas such as rectangular, triangular and elliptical disc monopoles [19].

6.2 Design Procedure

A rectangular planar monopole antenna can be assumed as a microstrip patch antenna with a ground plane at infinity [19]. Hence, air can be considered as the substrate since the majority of the space is air compared to thin substrate. The geometry of a rectangular planar microstrip antenna is depicted in Figure 6.2. In order to find the physical dimensions of rectangular planar monopole antenna equations (6.1) and (6.2) can be used [19].

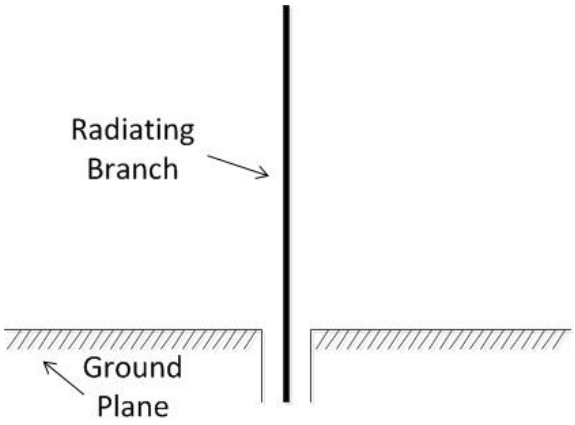

Figure 6.1. The geometry of a monopole antenna.

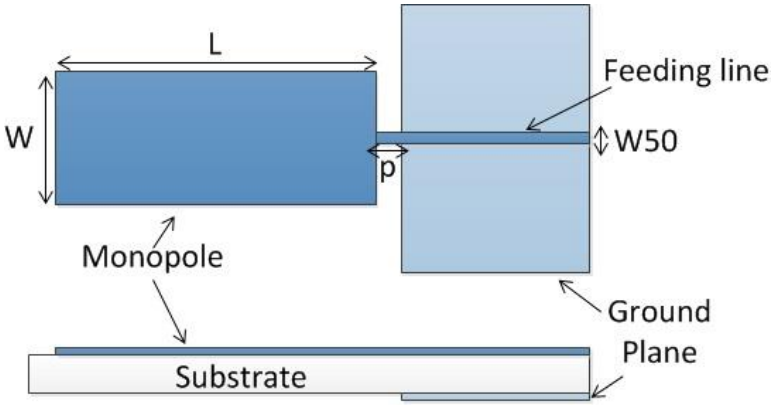

Figure 6.2. The geometry of a rectangular planar monopole antenna.

$$r = \frac{W}{2\pi} \quad (6.1)$$

$$f_L(GHz) = \frac{7.2}{L+r+p} \quad (6.2)$$

For W=60 mm, p=10 mm and f_L=600 MHz the obtained value for L is 100 mm. These values are utilized in the simulation software to check the input matching (S_{11}) of the antenna. Figure 6.3 shows the simulation results of S_{11} for different feeding line widths between 1 mm and 2 mm in the desired frequency interval. Comparing these results it can be deduced that for width equal to 1.6 mm the bandwidth and matching is the most suitable one. In the next step different values for the parameter p which affects the bandwidth and matching are simulated and the results are represented in Figure 6.4. Among these different values also p=6mm is chosen.

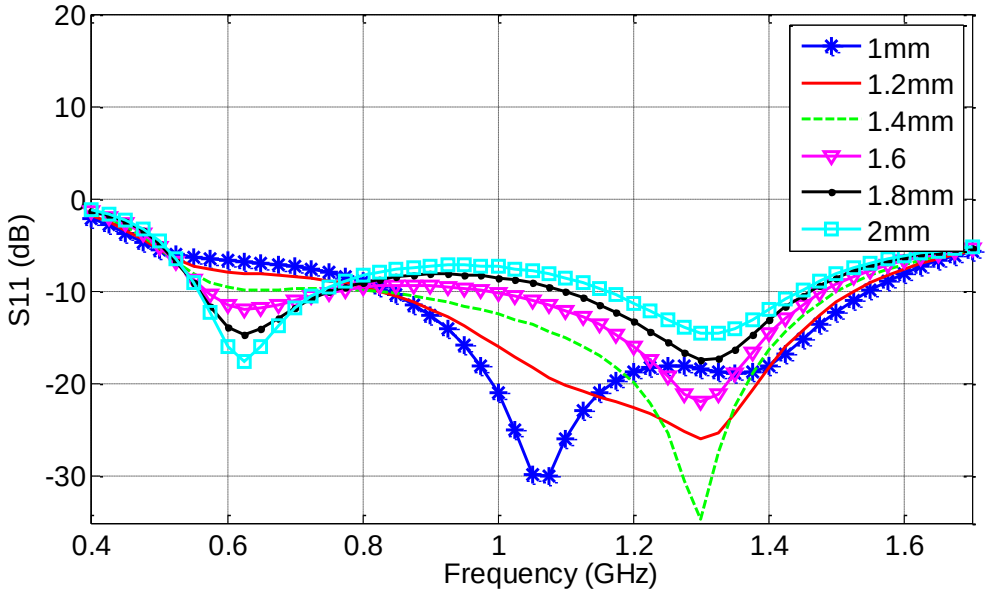

Figure 6.3. The simulation results of the proposed rectangular planar monopole antenna input matching for different values of W_{50}.

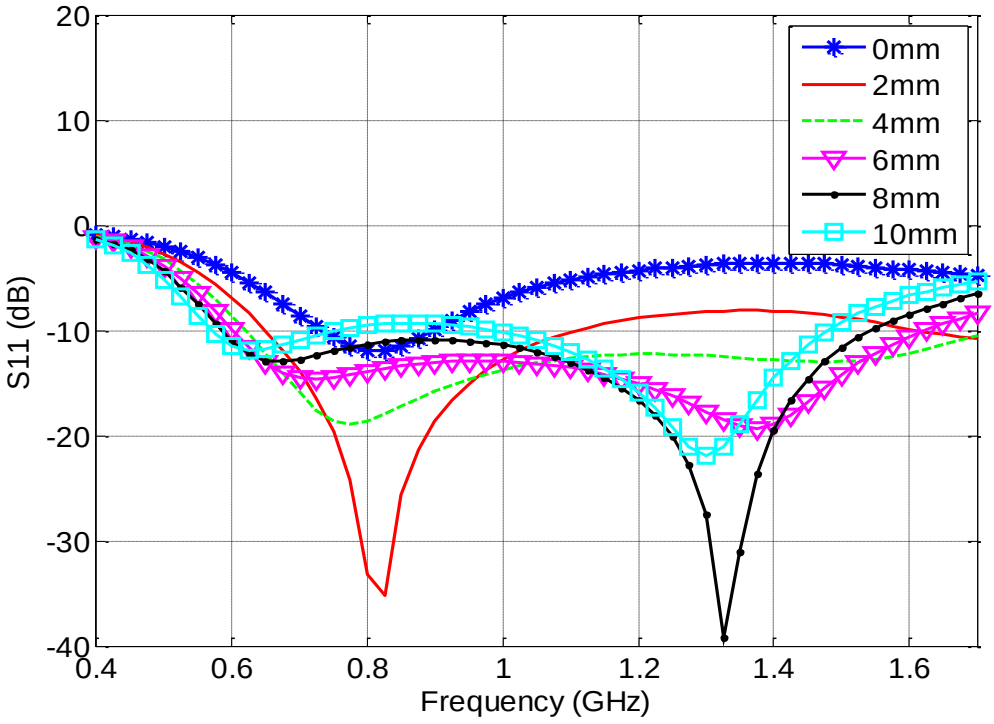

Figure 6.4. The simulation results of the input matching of the proposed rectangular planar monopole antenna for different values of *p*.

For the next step the feeding microstrip line is connected to the antenna using a tapered shape in order to improve the bandwidth and matching of the antenna [23], [24]. Having a tapered shape between the feeding line and the radiating part of antenna slightly transfers the impedance of the line to the impedance of antenna and reduces the reflections and mismatch. The proposed geometry and the simulation results are depicted

in Figure 6.5 and Figure 6.6, respectively. As can be seen, the bandwidth of the antenna is increased while the matching in some frequencies is worsened.

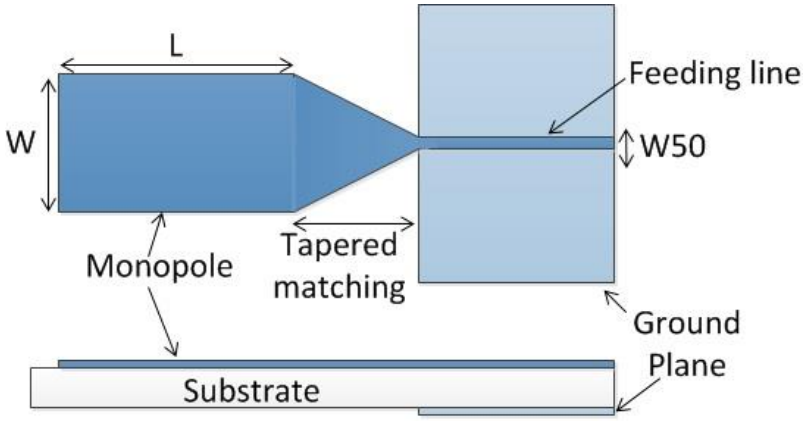

Figure 6.5. The geometry of the monopole antenna with tapered matching.

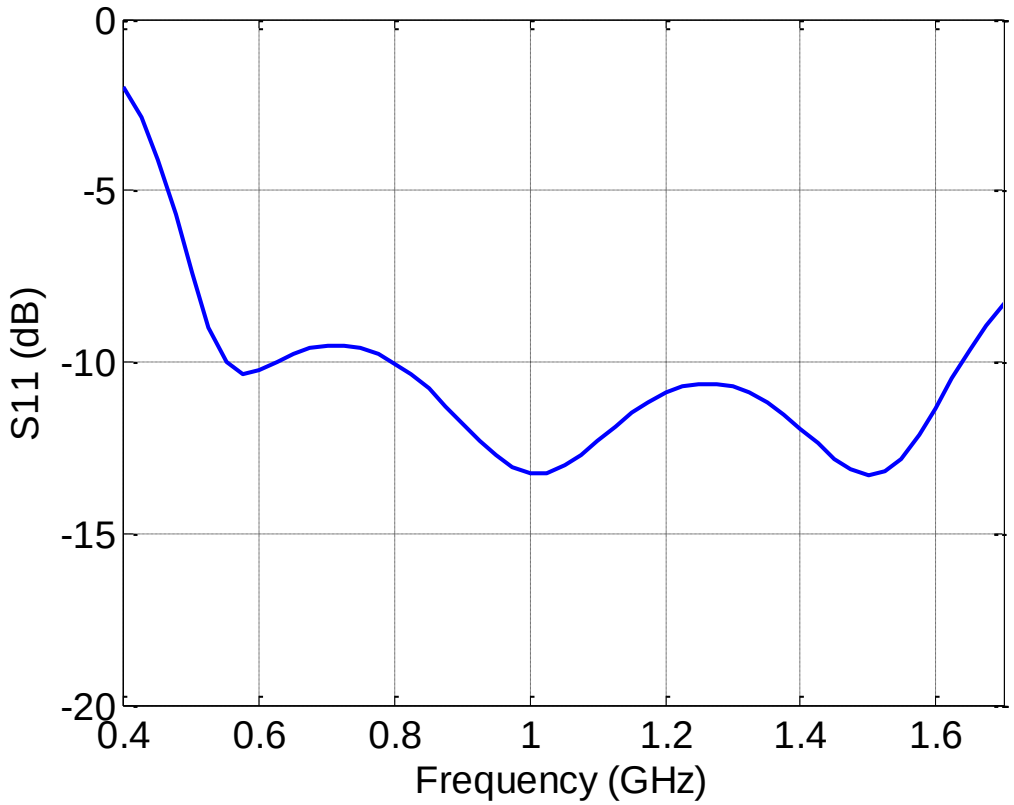

Figure 6.6. The simulation results of S_{11} of the monopole antenna with tapered matching.

For the last step, in order to improve the bandwidth and matching two slits are cut from the monopole pattern and one slit from the ground plane [23], [24], [25]. Therefore, by disturbing the current distribution and making different paths for current at different frequencies the desired performance can be achieved. The geometry and simulation results for the final design of the antenna and its simulation result are illustrated in Figure 6.7 and Figure 6.8, respectively. The accurate physical dimensions of the final design are presented in Table 3.

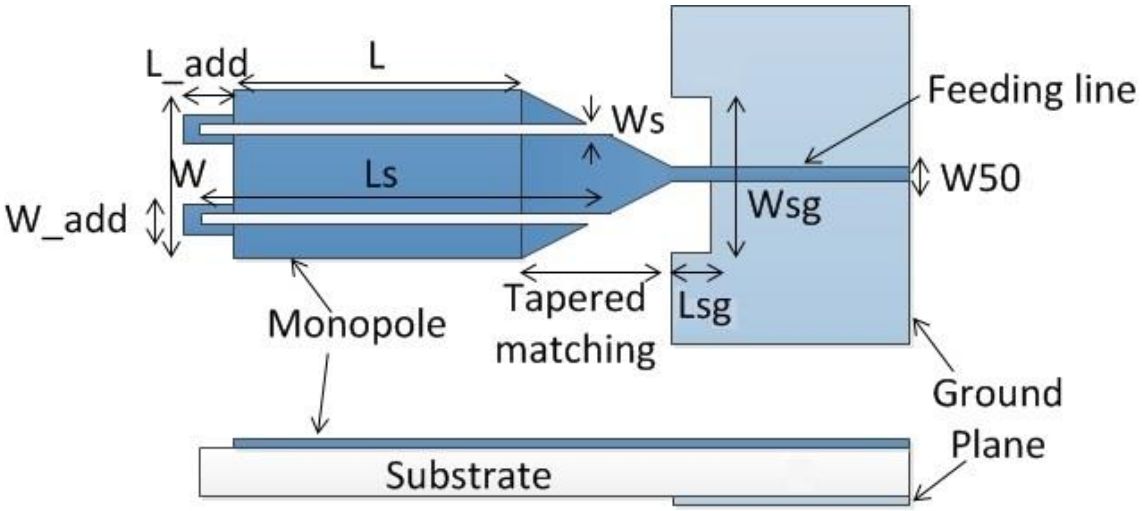

Figure 6.7. The final geometry of the proposed wide band monopole planar antenna.

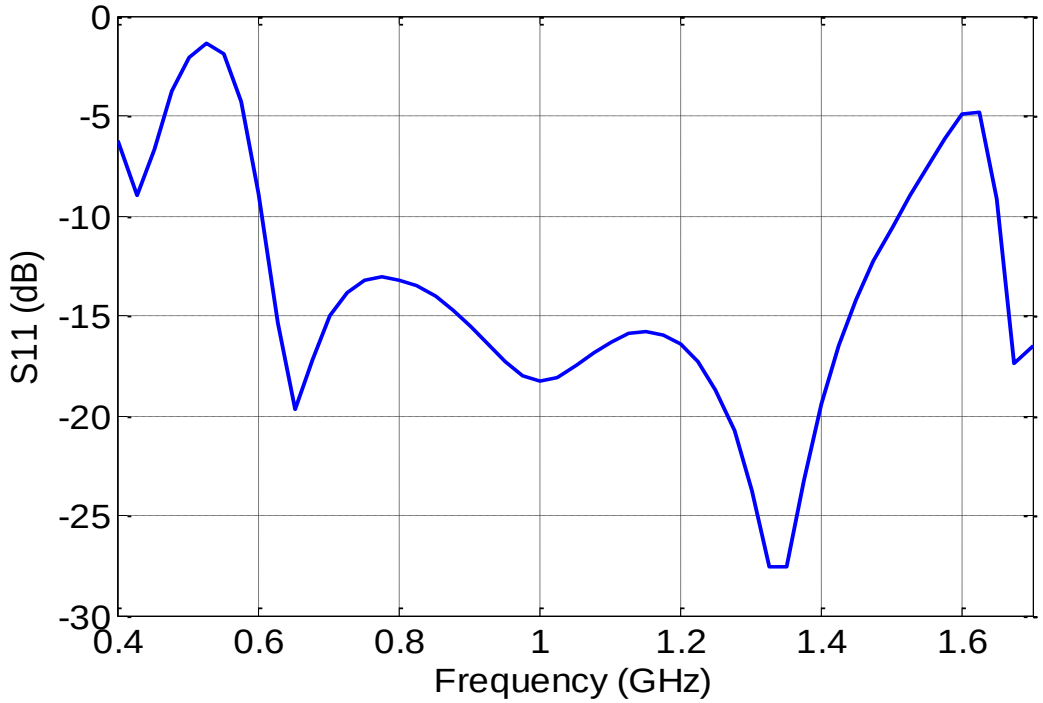

Figure 6.8. The simulation results for S_{11} of the proposed monopole antenna.

Table 3. The summary of the physical dimensions of the proposed wide band planar monopole antenna.

Parameter	L	W	Tappered Matching	W_{50}	L_s	W_s	L_{sg}	W_{sg}	L_{add}	W_{add}
Dimension (mm)	70	70	60	1	66	1	2	10	30	9

6.3 Simulation and Measurement Results

According to the aforementioned setting the proposed antenna is printed on cardboard after surface treatment. Figure 6.9 depicts the proposed inkjet-printed wideband planar monopole antenna.

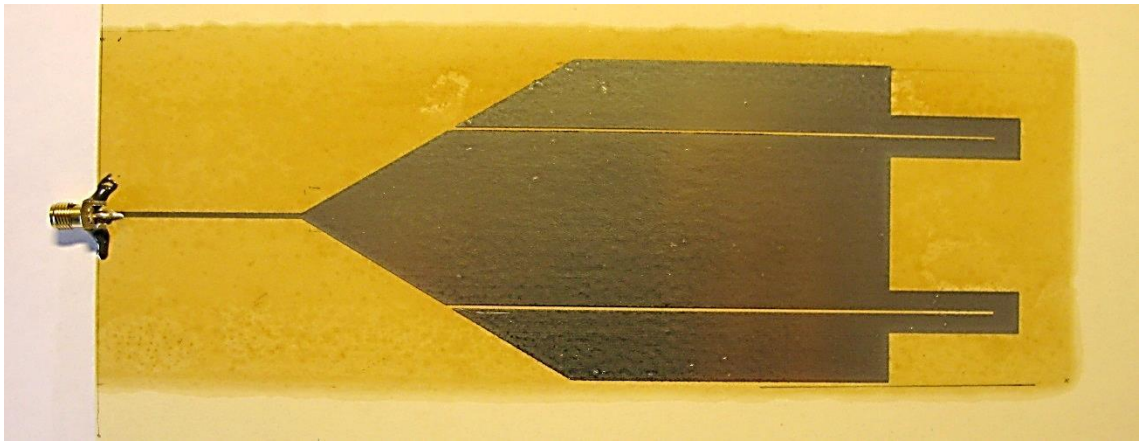

(a)

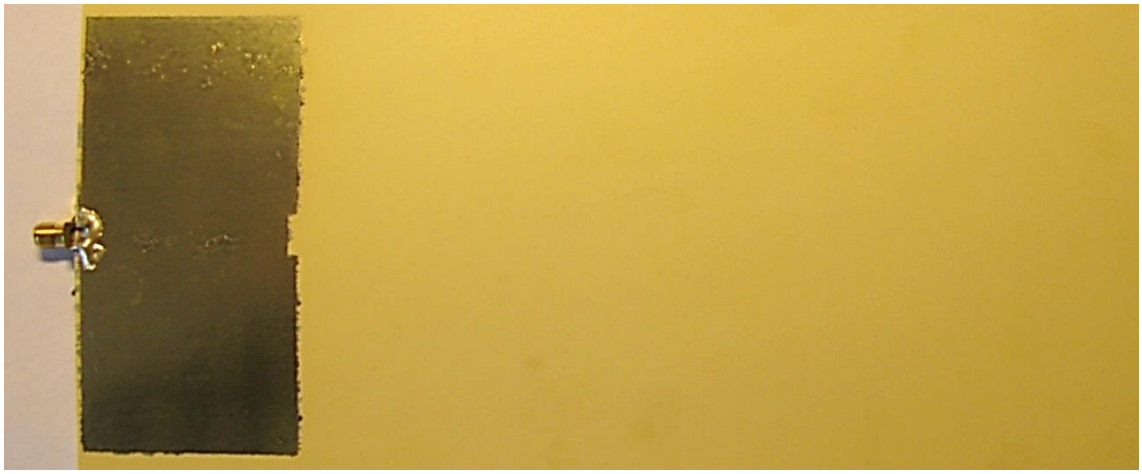

(b)

Figure 6.9. The inkjet-printed monopole antenna on cardboard. (a) Top view. (b) bottom view.

The simulation and measurement results for S_{11} of the proposed wide band planar monopole antenna are illustrated in Figure 6.10 . As can be seen, the results are in good agreement with each other. Figure 6.11 shows the simulation and experimental results of the maximum realized gain of the proposed antenna in the desired frequency interval, respectively. Because of the limitation in the operational frequency range of near-field measurement device (Satimo Starlab) it is not feasible to measure antenna parameters for frequencies lower than 800 MHz. Therefore, the gain and radiation patterns for lower frequencies are measured in the EMC chamber using far-field measurement techniques. Since this method is not as accurate as near-field measurement there are more inaccuracies in the results (at least 2-3 dBi in the gain). The simulation and measurement results for the total efficiency of the antenna can be seen in Figure 6.12. Since it is not possible to measure the total efficiency in the EMC chamber there is no information

for frequencies lower than 800 MHz. By comparing the simulation and measurement results of the maximum gain and total efficiency of the antenna it can be deduced that the antenna performs fine.

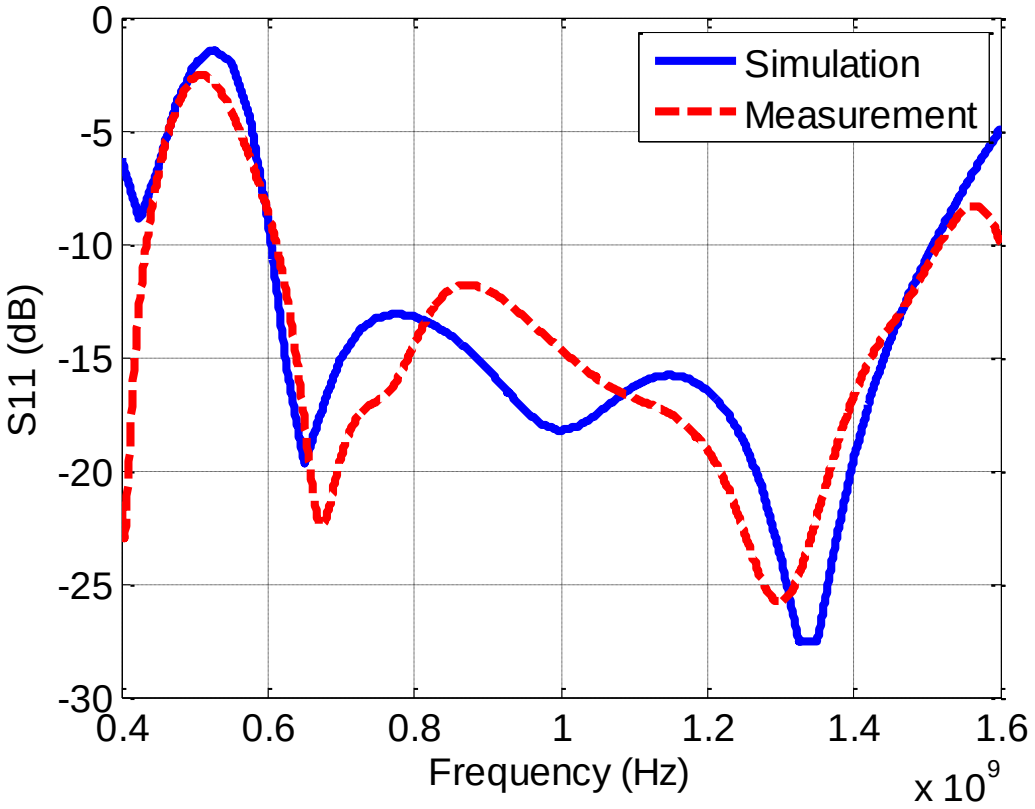

Figure 6.10. The simulation and measurement results of S_{11} for the inkjet-printed antenna.

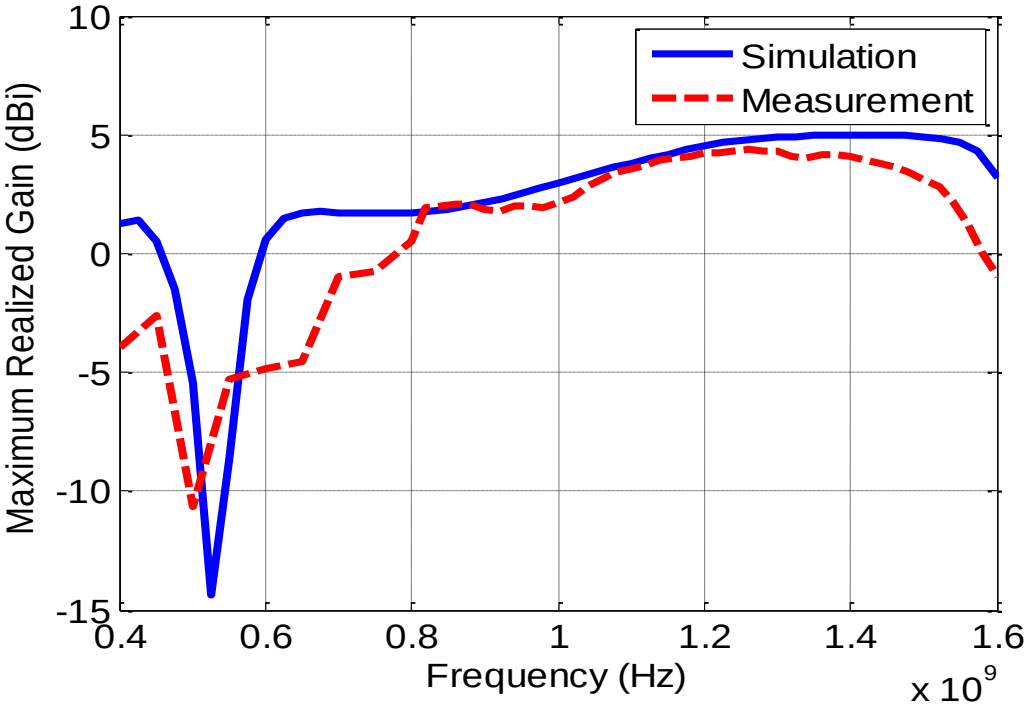

Figure 6.11. The simulation and measurement results for the maximum realized gain of the proposed antenna.

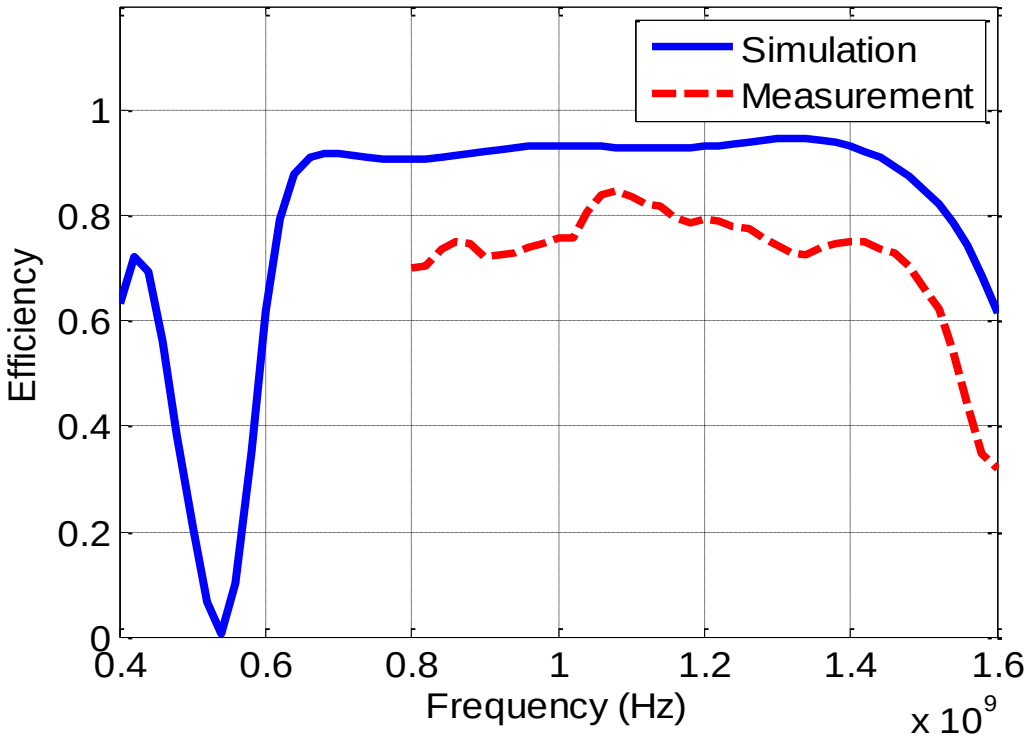

Figure 6.12. The simulation and measurement results for the total efficiency of the proposed antenna.

The other parameters which are beneficial to be investigated are the radiation patterns of the antenna. The simulation and measurement results of the E-plane and H-plane at different frequencies are presented in Figure 6.13. The measurement at 600 MHz is done in EMC-chamber and the rest in Satimo Starlab. As it was discussed before the measurement in EMC-chamber has more inaccuracies compared to Satimo Starlab. It can be seen that in most of these frequencies the results are in an acceptable range. The H-plane is omni-directional in the whole frequency interval. The E-plane is like ordinary monopole radiation patterns at lower frequencies while in higher frequencies the main beam is tilted toward the peak of the antenna and side lobes appears in the lower parts as it was expected.

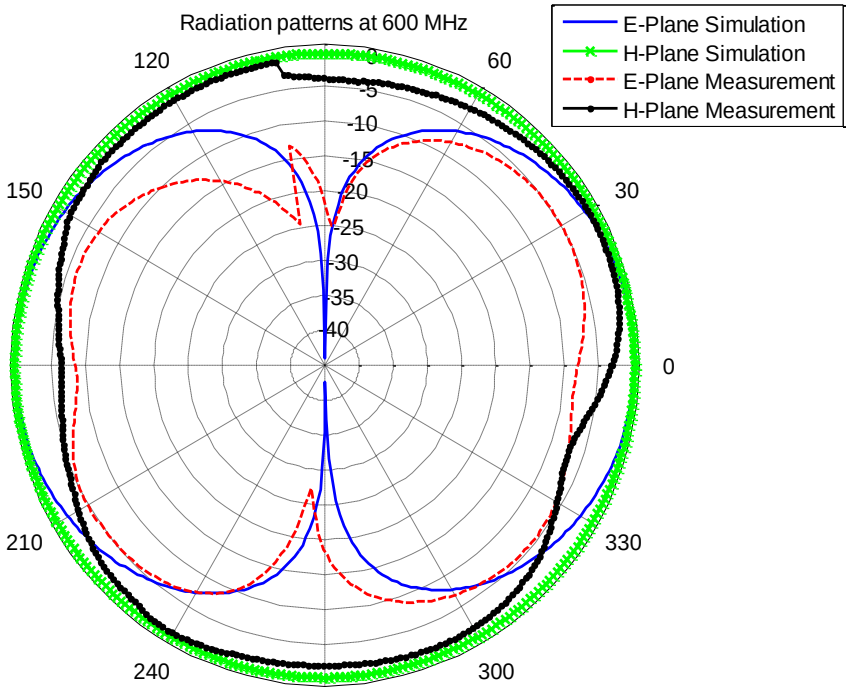

(a)

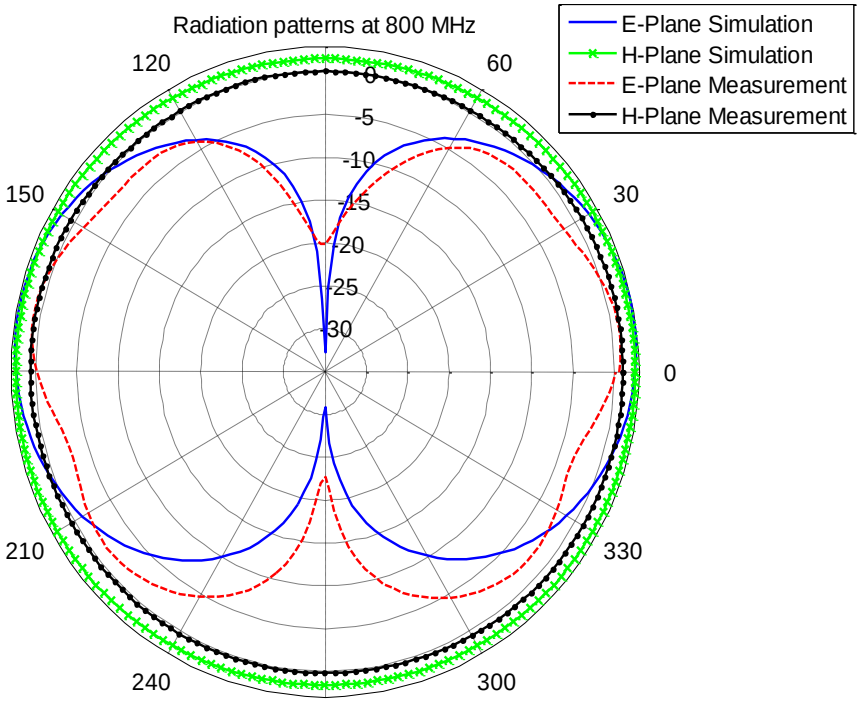
Radiation patterns at 800 MHz
E-Plane Simulation
H-Plane Simulation
E-Plane Measurement
H-Plane Measurement
120
60
150
30
0
210
330
240
300
0
-5
-10
-15
-20
-25
-30

(b)

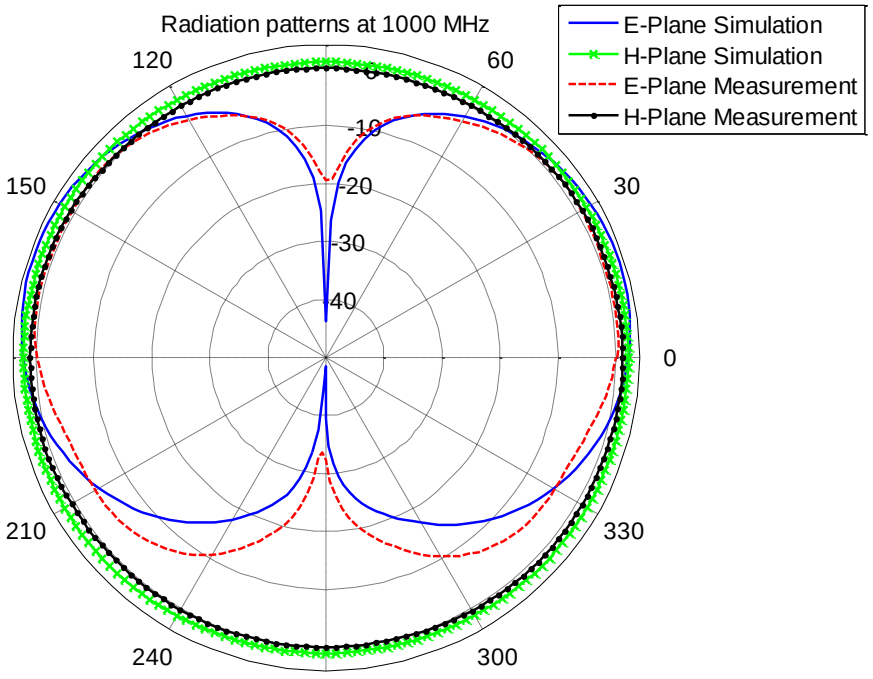
Radiation patterns at 1000 MHz
E-Plane Simulation
H-Plane Simulation
E-Plane Measurement
H-Plane Measurement
120
60
150
30
0
210
330
240
300
-10
-20
-30
-40

(c)

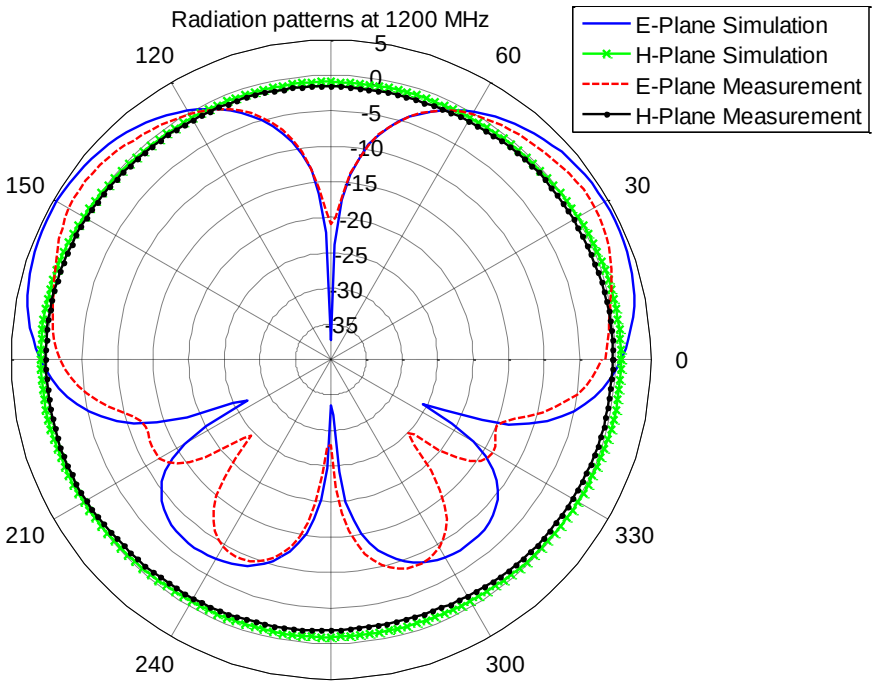

(d)

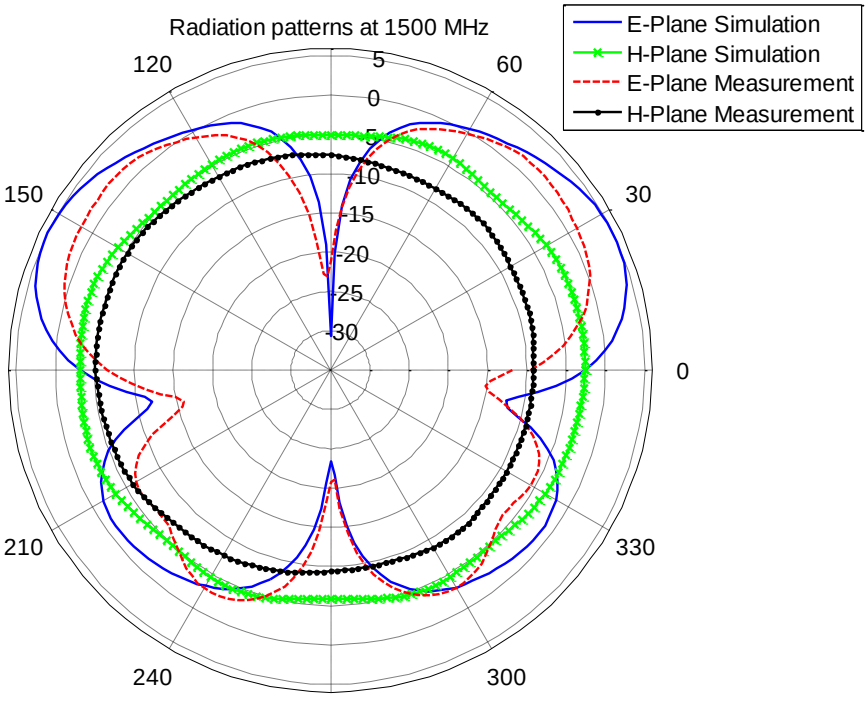

(e)

Figure 6.13. The simulation and measurement results of the radiation patterns for the proposed antenna at: (a) 600 MHz, (b) 800 MHz, (c) 1 GHz, (d) 1.2 GHz and (e) 1.5 GHz.

The current distributions at different frequencies are depicted in Figure 6.14. It can be seen that the maximum magnitude of the current appears around the two slits in the monopole structure and the slit in the ground plane in the whole operation frequency interval. In addition, the current distribution is relatively high in the outer part of the radiating edges which increase the radiation and bandwidth of the antenna.

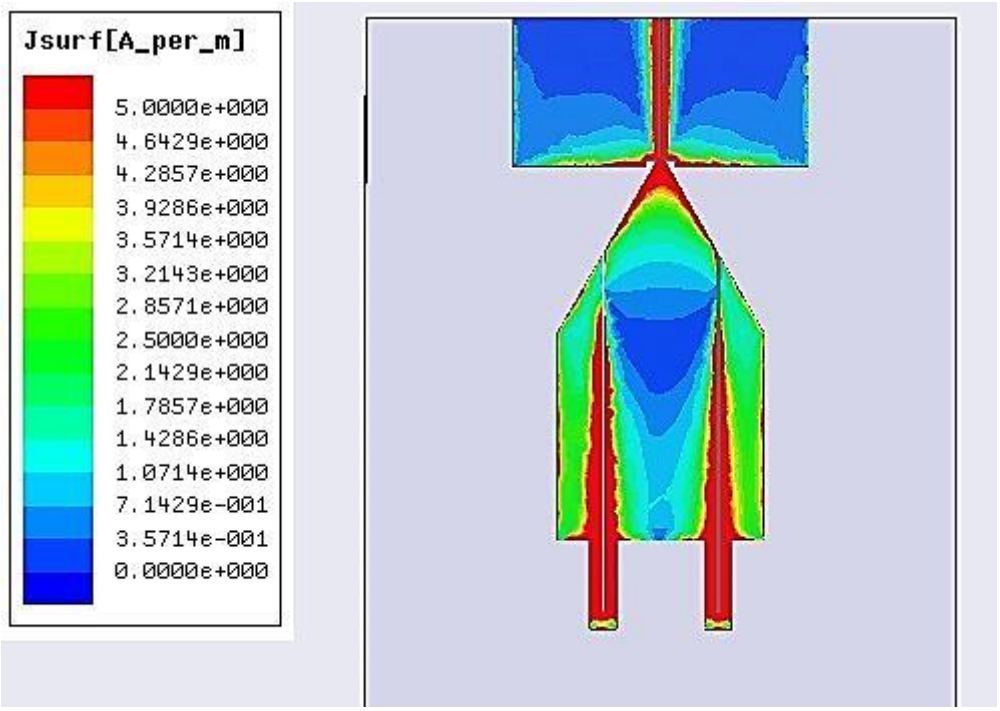

(a)

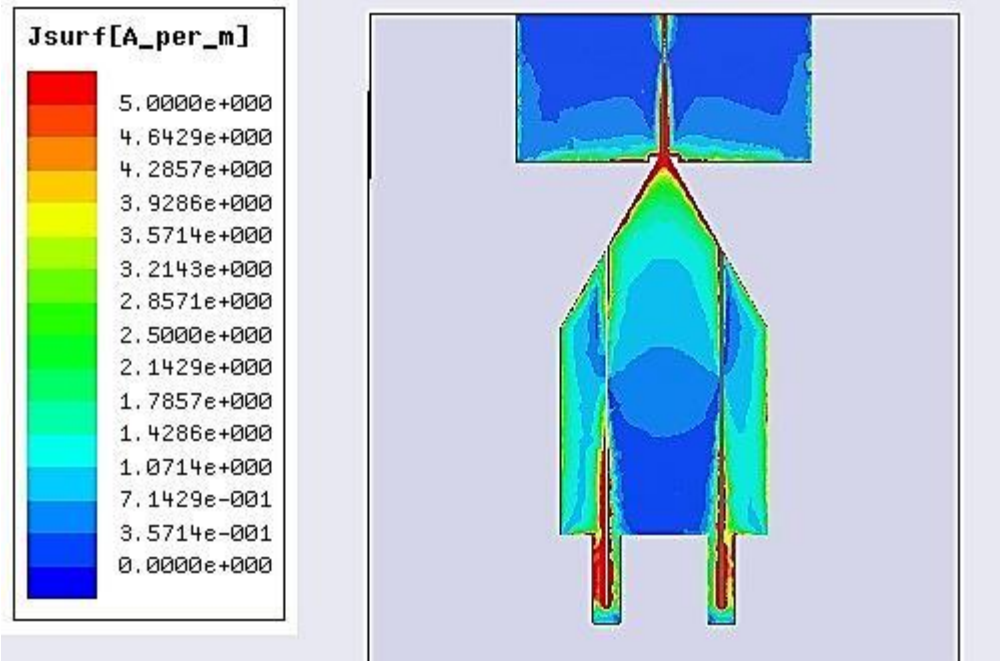

(b)

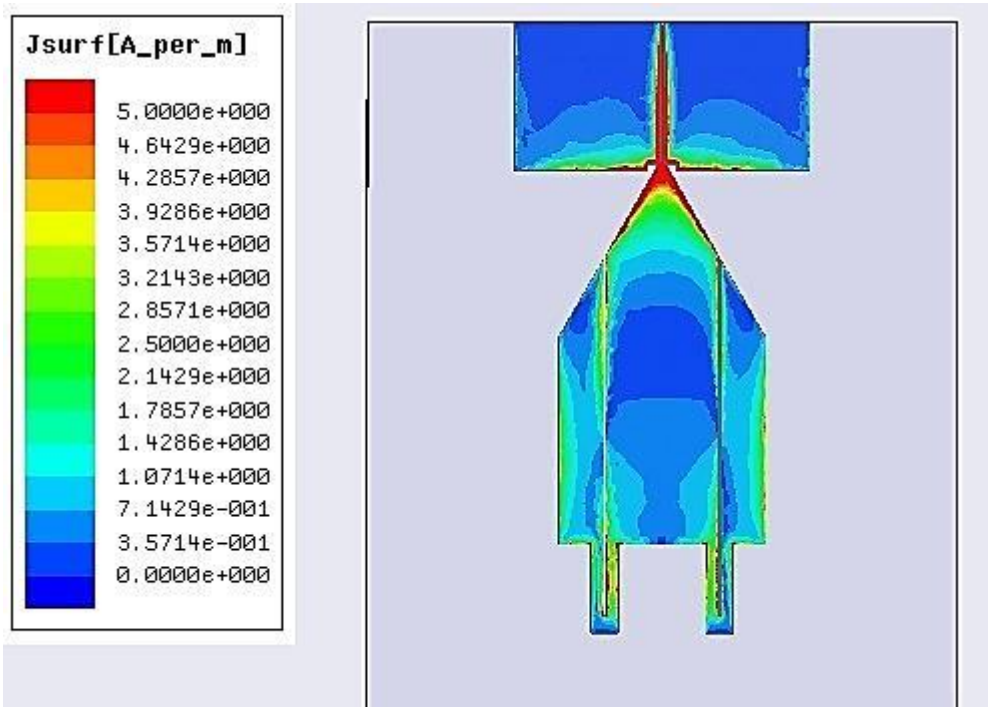

(c)

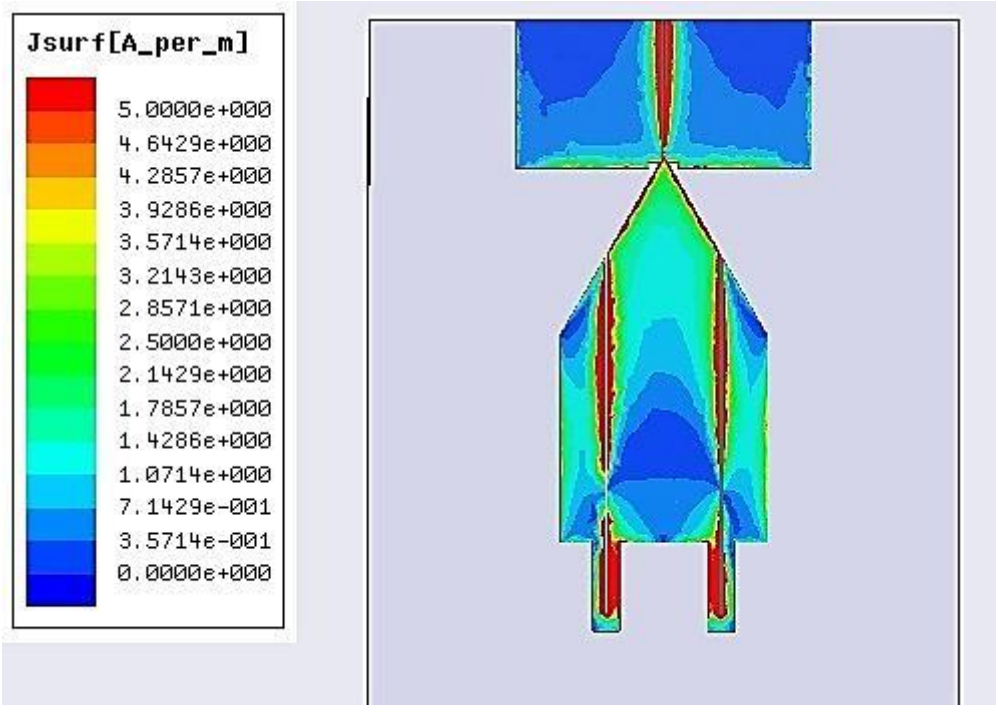

(d)

Figure 6.14. The current distribution in the proposed antenna structure at: (a) 600 MHz, (b) 800 MHz, (c) 1.2 GHz and (d) 1.5 GHz.

7. CONCLUSION

In this master's thesis, the design and development of a wide band antenna for power harvesting application using inkjet-printing technology on fibrous paper based substrates has been discussed. For this purpose the properties of the substrate and conductor were extracted in the desired frequency range using two-transmission line method and dielectric probe measurement. In order to check the reliability of the obtained parameters a band stop filter and microstrip patch antenna have been fabricated. Finally, a wide band antenna was designed and implemented on cardboard using inkjet-printing technology, then the simulation and measurement results are compared.

In order to find the permittivity and loss tangent of cardboard, identical microstrip lines with different lengths were implemented on cardboard using copper tape. Since the properties of the conductor are known in this scenario, the desired parameters for substrate can be achieved. In the next step in order to find the properties of printed silver traces, similar microstrip lines were implemented using inkjet-printing of silver ink. In this case the required parameters of substrate are known so the conductivity of silver traces can be obtained. Due to the fact that ink absorption by the substrate reduces the conductivity and efficiency of the circuits, a dielectric ink was utilized to make the surface of cardboard ink-proof and smooth. The obtained values for the permittivity, loss tangent of cardboard, and conductivity and thickness of printed silver traces are enough to design RF/Microwave circuits. The fabricated circuits using these values had identical performance compared to their simulation results.

The desired goal is the implementation of an inkjet-printed antenna on cardboard appropriate for power harvesting application. For the power harvesting block P2110 power-harvester is used; hence, the antenna specification should match with the power harvester. According to the desired specification a planar wideband monopole antenna was designed and fine-tuned. For this purpose, a simple rectangular planar monopole was chosen for the basis of the design. Its bandwidth and matching was improved by adding a tapered matching, two slits in the monopole structure, and one slit in the ground plane. Finally, the proposed antenna was implemented, measured and its performance was compared with the simulations. From the comparison it can be deduced that the antenna is operating desirably.

This project can be improved by implementing the whole paver harvester circuit and the sensor parts in the further studies.

8. PUBLICATIONS

- "Optimization of Inkjet Printing of Patch Antennas on Low-Cost Fibrous Substrates" Hossein Saghlatoon, Lauri Sydänheimo, Leena Ukkonen, Manos M. Tentzeris, IEEE Antennas and Wireless Propagation Letters, Dec 2013, (Accepted, minor revisions are needed)

- "Optimized RF/Microwave Antennas and Circuits on Low-Cost Fibrous Substrates Using Inkjet-Printing Technology" Hossein Saghlatoon, Lauri Sydänheimo, Leena Ukkonen, Manos M. Tentzeris, 2014 IEEE International Symposium on Antennas and Propagation AP-S 2014, Memphis, USA, (Accepted for oral presentation)

REFERENCES

[1] Palacios, S. Kim, S. Elia, S. Rida, A. Tentzeris, M.M. Nikolau, S. Inkjet–Printed Planar Antenna for a Wireless Sensor on Paper Operating at Wi-Fi Frequency. Antennas and Propagation Society International Symposium (APS/URSI), July 2012. IEEE. p 1-2.

[2] Irimia-Vladu, M. 2014. Green Electronics: Biodegradable and Biocompatible Materials and Devices for Sustainable Future. Chemical Society Reviews, 43(2), p 588-610.

[3] Yang, L. Rida, A. Vyas, R. Tentzeris, M.M. RFID Tag and RF Structures on Paper Substates Using Inkjet-Printing Technology. IEEE Transactions on Microwave Theory and Techniques 55(2007)12 part2, p. 2894-2901.

[4] Virkki, J. Virtanen, J. Sydanheimo, L. Ukkonen, L. Tentzeris, M.M. 2012. Embedding Inkjet-Printed Antennas into Plywood Structures for Identification and Sensing. RFID-Technologies and Applications (RFID-TA), 2012 IEEE International Conference. IEEE. p 34-39.

[5] Babar, A.A. Virtanen, J. Bhagavati, V.A. Ukkonen, L. Elsherbeni, A.Z. Kallio, P. Sydanheimo, L. 2012. Inkjet-Printable UHF RFID Tag Antenna on a Flexible Ceramic-Polymer Composite Substrate. Microwave Symposium Digest (MTT), 2012 IEEE MTT-S International. IEEE. p 1-3.

[6] Din, N. M., Chakrabarty, C. K., Ismail, A. B., Devi, K. K. A., & Chen, W. Y. 2012. Design of RF Energy Harvesting System for Energizing Low Power Devices. Progress In Electromagnetics Research. p 132.

[7] Tentzeris, M. M. Kawahara, Y. 2008. Novel Energy Harvesting Technologies for ICT Applications. In Applications and the Internet, SAINT 2008. International Symposium. IEEE. p 373-376).

[8] Cheng, D.K. Field and Wave Electromagnetics. Second Edition. The USA, Addison-Wesley Publishing Company. 1992. 674 p.

[9] Kraus, J.D. Fliesch, D.A. Electromagnetics with Applications. 5th Edition. The USA, McGraw-Hill. 1999

[10] Pozar, D.M. Microwave Engineering. The USA, Addison-Wesley Publishing Company. 1990. 719 p.

[11] Kraus, J.D. Antennas for All Applications. 3rd Edition. The USA, McGraw-Hill. 2002. 921 p.

[12] Balanis, C.A. Antenna Theory Analysis and Design. 2nd Edition. The USA, John Wiley & Sons, Inc. 1997. 931 p.

[13] Stutzman, W.L. Thiele, G.A. Antenna Theory and Design. 2nd Edition. The USA, John Wiley & Sons, Inc. 1998. 643 p.

[14] Virtanen, J. 2012. Development of Sensor Integrated and Inkjet-Printed Tag Antennas for Passive UHF RFID Systems. Dissertation. Tampere. Tampere University of Technology. Department of Electronics, Publication 1098. p 67.

[15] Hon, K.K.B, Li, L. Hutchings, I.M. 2008. Direct Writing Technology-Advances and Developments. CIRP Annals-Manufacturing Technology 57, 2, p 601-620.

[16] Saghlatoon, H. Sydänheimo, L. Ukkonen, L. Tentzeris, M.M. Optimization of Inkjet Printing of Patch Antennas on Low-Cost Fibrous Substrates. IEEE Antenna and Wave Propagation Letter. (submitted) Dec 2013.

[17] Chang, S.H. Kuan, H. Wu, H.W. Yang, R.Y. Weng, M.H. 2006. Determination of Microwave Dielectric Constant by Two Microstrip Line Method Combined with EM Simulation. Microwave and Optical Technology Letters 48, 11, pp. 2199-2201.

[18] Denneulin, A. Bras, J. Blayo, A. Neuman, C. Substrate Pretreatment of Flexible Materials for Printed Electronics with Carbon Nano Tube Based Ink. Applied Surface Science 257 (2011) 8, p. 3645-3651.

[19] Kumar, G. Ray, K.P. Broadband Microstrip Antennas. The UK, Artech House, Inc. 2003. p 409.

[20] Bahl, I.J. Bhartia, P. Microstrip Antennas. Dedham, MA. Artech House, Inc. 1980.

[21] Pozar, D.M. Schaubert, D.H. Microstrip Antennas: The Analysis and Design of Microstrip Antennas and Arrays. The USA. IEEE Press. 1995

[22] Lee, H.E. Chen, W. Advances in Microstrip and Printed Antennas. The USA. John Wiley & Sons, Inc. 1997.

[23] Eldek, A. A. 2006. Numerical analysis of a small ultra wideband microstrip-fed tap monopole antenna. Progress In Electromagnetics Research, 65, p 59-69.

[24] Eldek, A. A. 2006. A small ultra-wideband planar tap monopole antenna with slit, tapered transition, and notched ground plane. Microwave and optical technology letters, 48(8), p 1650-1654.

[25] Jung, J. Choi, W. Choi, J. 2005. A small wideband microstrip-fed monopole antenna. IEEE Microwave and Wireless Components Letters, 15(10), p 703-705.